REPORT DOCUMENTATION PAGE	Form Approved OMB No. 0704-0188

1. AGENCY USE ONLY *(Leave blank)*	2. REPORT DATE	3. REPORT TYPE AND DATES COVERED
	30.Oct.00	THESIS

4. TITLE AND SUBTITLE
DECOMPOSED ANALYSIS OF THE RELIABILITY OF AREA-ARRAY ELECTRONIC PACKAGES INCLUDING ASSEMBLY PROCESS EFFECTS

5. FUNDING NUMBERS

6. AUTHOR(S)
MAJ THOMPSON TERRACE B

7. PERFORMING ORGANIZATION NAME(S) AND ADDRESS(ES)
UNIVERSITY OF COLORADO AT BOULDER

8. PERFORMING ORGANIZATION REPORT NUMBER
CY00398

9. SPONSORING/MONITORING AGENCY NAME(S) AND ADDRESS(ES)
THE DEPARTMENT OF THE AIR FORCE
AFIT/CIA, BLDG 125
2950 P STREET
WPAFB OH 45433

10. SPONSORING/MONITORING AGENCY REPORT NUMBER

11. SUPPLEMENTARY NOTES

12a. DISTRIBUTION AVAILABILITY STATEMENT
Unlimited distribution
In Accordance With AFI 35-205/AFIT Sup 1

12b. DISTRIBUTION CODE

13. ABSTRACT *(Maximum 200 words)*

14. SUBJECT TERMS	15. NUMBER OF PAGES	16. PRICE CODE
	120	

17. SECURITY CLASSIFICATION OF REPORT	18. SECURITY CLASSIFICATION OF THIS PAGE	19. SECURITY CLASSIFICATION OF ABSTRACT	20. LIMITATION OF ABSTRACT

Decomposed Analysis of the Reliability of Area-Array Electronic Packages Including Assembly Process Effects

by

Terrace Barrell Thompson

B.S., Virginia Military Institute, 1985

M.S., Boston University, 1992

A thesis submitted to the

Faculty of the Graduate School of the

University of Colorado in partial fulfillment

of requirements for the degree of

Doctor of Philosophy

Department of Mechanical Engineering

2000

This thesis entitled:
Decomposed Analysis of the Reliability of Area-Array Electronic Packages
Including Assembly Process Effects
written by Terrace Barrell Thompson
has been approved for the Department of Mechanical Engineering

Ganesh Subbarayan

Yung-Cheng Lee

Date 9 Oct 00

The final copy of this thesis has been examined by the signatories, and we find that both the content and the form meet acceptable presentation standards of scholarly work in the above-mentioned discipline.

Thompson, Terrace Barrell (Ph. D., Mechanical Engineering)

Decomposed Analysis of the Reliability of Area-Array Electronic Packages Including Assembly Process Effects

Thesis directed by Associate Professor Ganesh Subbarayan

The research presented in this thesis focuses on the use of a decomposed analysis technique to assess the reliability impact on area-array packages due to assembly process effects. The developed models enable one to determine the equilibrium configuration of electronic packages with warped and non-warped solder joints with significant computational efficiency at a reasonable accuracy. The code described herein uses a nonlinear optimization procedure that ensures the approximate satisfaction of the energy balance equation. The developed procedure is demonstrated on two- and three-dimensional hypothetical and "real-world" electronic packages with warped and non-warped solder joints. It is shown that with the use of the decomposed solution methodology, for a 225 I/O PBGA package with non-warped solder joints, a speedup of nearly seven times is achieved at an accuracy loss in displacements of approximately 5.46%. Since the analysis procedure is independent of the number of solder interconnects, significantly larger timesavings are expected for larger packages.

One ultimate utility of any technique employed to analyze electronic packages is to assess package reliability. Reliability assessment techniques normally consist of three basic steps to calculate (Subbarayan, et al., 1996):

1. solder joint shapes,

2. thermal stress/strain distribution in the most susceptible joint after solidification and during thermal cycling, and

3. fatigue lives of the most susceptible or any other selected solder joints.

For step one, we will demonstrate a novel methodology for studying the effect of printed circuit board (PCB) warpage and solder joint volume variation on the final equilibrium configuration of area-array packages. The effect of warpage is analyzed using a two-step procedure. In the first step, the restoring forces and moments (in the molten state of solder droplet) that result from a given solder joint height, solder material volume, pad diameter, and pad tilt are predicted using the surface tension theory. In the second step of the analysis, the forces and moments at individual solder joints caused by varying solder heights, pad tilts, and solder volume are combined using an optimization procedure to predict the equilibrium configuration of the package.

The developed procedure is demonstrated on a hypothetical area-array package with nine solder joints. Through an analysis of two scenarios for the hypothetical array: 1) constant solder volume with symmetric and non-symmetric package warpage, and 2) linearly distributed solder volume without warpage, it is shown that printed circuit board warpage can cause packages to tilt during solder reflow resulting in variations in solder joint heights and pad tilts.

For step two in assessing package reliability, namely thermal stress/strain distribution, we will combine the decomposition based analysis technique and the methodology for predicting the equilibrium configuration of warped electronic

packages to study the reliability impact of warped solder joints in area-array packages. The methodology is developed and demonstrated on a hypothetical area-array package with four warped solder joints. An assumption that enabled computational efficiency was that the geometrical change (to the nominal geometry) caused by warpage of the component/PCB did not significantly alter the stiffness of the structure. This allowed the use of substructure models of the component/PCB together with accurate models of individual solder joints with widely varying shapes in the decomposed analysis procedure.

It is shown that the use of the decomposed solution methodology for analyzing a package with warped solder joints leads to an overall accuracy loss in relative shear displacements of approximately 7.18 percent. This error translates to an accuracy loss in fatigue life calculation of approximately 11.83 percent. A comparison of the reliability of a package with warped and non-warped joints reveals package tilt due to solder volume variation and/or non-symmetric warpage can change the stand-off height of solder joints profoundly affecting solder joint reliability. However, we found that individual solder pad tilts in a range from 0 to 3 degrees, independent of solder standoff height, do not affect the reliability of solder joints.

Acknowledgements

I would like to express my deepest thanks to my advisor, Professor Ganesh Subbarayan, for his endless support, encouragement, and guidance during the course of my research. Without his assistance, my work, if even possible, would have been much more difficult and much less enjoyable.

I would also like to thank Professors K. C. Gupta, Jack Zable, Yung-Cheng Lee, and Lawrence Carlson for their support, advice, and specifically serving on my thesis defense committee.

The current and former members of Ganesh Subbarayans's research group and students in other research groups that I have had the pleasure to work with have made my work always interesting, exciting, and enjoyable.

Without financial support, none of this work would have been possible. I would like to thank the United States Air Force , United States Air Force Academy, and Air Force Institute of Technology for allowing me the opportunity to participate in the Ph. D. program. In addition, I would like to acknowledge the Semiconductor Research Corporation under contract number PJ 607 and task id 603.001 and the National Science Foundation under contract ECS 9734349. The authors are also thankful to Professor K. Schittkowski from the University of Bayreuth, Germany, for allowing access to the NLPQL code.

Continued participation in the Ph. D. program would not have been possible without the continuous support and encouragement of my family. When days appeared cloudy and gray, they always brought sunlight to my life.

Lastly and most importantly, I would like to thank my Lord and Saviour, Jesus Christ. He heard and answered and my prayers.

Contents

Figures

Figure

Tables

Table

Chapter 1

Introduction

1.1 Decomposition

Engineering systems, in general, are physically challenging to model and computationally expensive to simulate. Electronic packages are excellent examples of complex engineering systems since they involve multiple physical domains, namely electrical, mechanical, and thermal and complexity within each domain. The analysis complexity arises out of factors such as: nonlinear behavior of materials (e.g., plastic and creep deformations of solder), complex package construction, and the large number of interconnections. As electronic packages increase in size and density, common analysis techniques such as finite element (FE) analysis have become very inefficient for these systems and are too slow for quick design decisions. Optimal design of electronic packages is even more expensive since optimization techniques are iterative in nature and each iteration, using FE analysis, would require regeneration of the FE mesh (for the new geometry) prior to re-analysis. The need for efficient as well as accurate techniques for analysis and

design of complex mechanical systems in general and electronic packages in particular are obvious.

A brief background on the methodology developed by Deshpande and Subbarayan (1999) as it relates to the present research is described below. In general, the finite element method is a popular choice for the analysis of microelectronic packages. The concept of a superelement is well established in the finite element method, where a global stiffness matrix is partitioned into retained and eliminated portions (referred by subscripts *r* and *e* below) as follows:

$$\begin{bmatrix} \mathbf{K}_{rr} & \mathbf{K}_{re} \\ \mathbf{K}_{re} & \mathbf{K}_{ee} \end{bmatrix} \begin{Bmatrix} \mathbf{u}_r \\ \mathbf{u}_e \end{Bmatrix} = \begin{Bmatrix} \mathbf{f}_r \\ \mathbf{f}_e \end{Bmatrix} \tag{1.1}$$

$$\begin{aligned} \tilde{\mathbf{K}}_{rr}\mathbf{u}_r &= \tilde{\mathbf{f}}_r \\ \tilde{\mathbf{K}}_{rr} &= \mathbf{K}_{rr} - \mathbf{K}_{re}\mathbf{K}_{ee}^{-1}\mathbf{K}_{er} \\ \tilde{\mathbf{f}}_r &= \mathbf{f}_r - \mathbf{K}_{re}\mathbf{K}_{ee}^{-1}\mathbf{f}_e \end{aligned} \tag{1.2}$$

The concept of superelements in finite element analysis allows the partitioning of a large linear structure into substructures for ease of analysis (see for example, Zienkiewicz and Taylor, 1990). When two superelements are "connected", the mesh or the nodal degrees of freedom at the interface must match. Also, superelements are valid only for linear systems since they rely on the idea of a constant stiffness matrix. Thus, their applicability to microelectronic packages is limited since solder alloys and other materials commonly used are known to behave nonlinearly. The decomposition methodology extends the concept of superelement by allowing for mesh mismatch between the substructures at the interface, and by allowing nonlinearly behaving substructures.

The earlier derived theoretical methodology of Deshpande and Subbarayan (1999) were validated in their work using a code developed specifically for the analysis of the 5x5 array used in that study. Any change in package configuration or construction requires a considerable amount of reprogramming and debugging. The application and demonstration of a code, based on the decomposition procedure and assumed displacements fields, to hypothetical and "real-world" electronic packages is one of the goals of the current research. By simply modifying the code input deck to account for new package geometries, we were able to analyze new electronic packages with ease.

1.2 Assembly Process-Induced Variations in Array-Packages

The current trends in the electronic packaging industry are toward larger packages, increased density, new substrate materials and new printed circuit board (PWBs) constructions. This has led to issues with PWB and component warpage which is believed to lead to component misalignment and/or tilt during solder reflow processes resulting in a premature solder joint failure during use conditions. There is a need to systematically study the reliability implications of symmetric and non-symmetric circuit board/component warpage and solder volume variation in electronic packages since it is believed that these variations could lead to non-intuitive failures in joints other than the usual "corner joint" at the die edge.

1.3 Literature Review

1.3.1 Decomposition in Electronic Packages

Deshpande accomplished much of the literature review on domain and design composition during his Ph. D. research. The application of decomposition-based finite element analysis to electronic packages is novel work and Deshpande (1999) presents the only literature found on the application of these techniques for efficient analysis of electronic packages.

Cheng, et al., (1998) present an efficient method for FE analysis of BGA packages. Their method is based on replacing solder joints by equivalent beams and calculating the properties of the equivalent beam using a designed experiment based on analyses of 3-D solder models. Once the equivalent beam is formulated they perform a full 3-D FE analysis of the entire package using the equivalent beam. The methodology is not decomposition based since the component and PWB are not separate subsystems, thus any changes in either would require a complete re-analysis of the 3-D model with the beams. The decomposition methodology is free from this limitation.

Saito, et al., (1999) also present an efficient stress and displacement analysis method for area-array structures based on the equivalent beam methodology where two-node beam elements with stiffness matrices extracted from load-displacement relationships are used to model the solder joints and shell elements are used to model the package and PWB. This method has the same limitation as Cheng's method above.

Darbha and Dasgupta (1999) present a stress analysis technique for electronic packages based on a nested finite element methodology (NFEM) where colonies of nested sub-elements are created inside a main element to capture localized large gradients of stress and strain. The nesting concept reduces the number of degrees of

freedom of the FE model, thus reducing computational time since the nested finite elements are only developed for critical regions of the package. Once again, this methodology is not decomposition based since any design change would require re-analysis of a full 3-D finite element mesh.

1.3.2 Warpage in Electronic Packages

A large body of literature is published on warpage in electronic packages and its effect on solder joint reliability. Most of the literature is aimed at doing one of three things:

1. Development of methodologies to predict warpage of electronic packages with or without analysis to determine solder joint reliability.
2. Development of techniques to provide "real-time" monitoring of warped electronic packages pre, in-situ, or post-assembly in order to determine solder yield, where the yield criteria is based on a maximum/minimum solder joint height that would cause an open or short circuit.
3. Development of techniques to predict the shape and yield/reliability of solder joints in warped electronic packages.

Amagai (1999) found that package warpage tremendously affected solder joint reliability in Chip Scale Packages. The effect of molding compound and die attach film on package warpage was investigated using 3-D non-linear (viscoplastic and viscoelastic) finite element analysis. Amagai was able to correlate the magnitude of package warpage after encapsulation to solder fatigue life. Thermal cycling of the 3-D finite element models and subsequent fatigue life calculations

showed the solder joints near the chip edge of the package with the greatest warpage failed first.

Yao and Qu (1999) investigated the effect of printed wiring board size on the overall deflection of flip-chip assemblies and found that the size of the PWB had significant implications on the design of multi-chip modules (MCMs). Three-dimensional finite element analyses were used to study the stress distribution in and deflection of the flip chip assembly. The FE model was validated with experimental results of stress distribution. The results indicate that a square array placement pattern is preferable to a staggered array for MCMs and a minimum distance between adjacent dies should be approximately 2 times the die size in order to reduce mechanical interaction between chips.

He, X. and Lu, S. (1998) present and demonstrate a new portable projected grating moiré system. The system was designed and built for component level warpage measurement and allows precision measurement of warpage, providing valuable insight into package reliability, manufacturing process and model validation. Verma, et al., (1998) developed a compact apparatus combining far infra-red Fizeau interferometry and shadow moiré with enhanced sensitivity methodologies to measure real-time warpage with a variable sensitivity ranging from 2.5 μm to 100 μm.

Lee (1997) developed an analytical model to the study warpage of plastic ball-grid-array packages under uniform thermal loading. The model was derived from the classical laminated plate theory. A series of parametric studies were performed to investigate the effects of chip size, chip thickness, BT substrate

thickness, and molding compound thickness on package warpage. The model provides the packaging engineer with a convenient tool to evaluate PBGA warpage.

Egan, et al., (1998) described the overall warpage of a PBGA package as consisting of two curvatures, a die-area curvature and a mold-area curvature. This was based on measurements done on physical samples of PBGAs. An analytical expression for dual-curvature beam bending is developed and compared with previous predictions for multi-layered beam bending and 3-D finite element analysis. The dual-curvature approach yielded very good 2-D accuracy and fairly good 3-D accuracy.

In all of the above research, solder joint shape prediction and the reliability resulting from warped circuit boards and packages has not received much attention. Ju et al., (1994), Chan et al., (1997), and Tower, et al., (1999) appear to be the only studies of this nature.

Ju et al., (1994) studied the effects of manufacturing variations on the reliability of solder joints between a ceramic ball grid array (CBGA) electronic package and PWB. Manufacturing variations considered included changes in solder volume, joint height, and pad size, where the joint height variation was caused by the package warpage. They investigated the effect of spacers to model warpage and control solder joint height and compared the fatigue life of the package outermost corner joint's convex (truncated sphere shaped), cylindrical or concave (hour-glass shaped) profiles produced by these spacers. Solder life prediction calculations showed concave solder joints had long fatigue lives and were less sensitive to manufacturing variations when the spacers were used. They concluded the reliability of convex solder joints is significantly affected by the height variations

associated with the package warpage. More than 50 percent variation in lives estimated for a +/- 10 percent height change.

Chan, et al., (1997) established a reliability model to study thermal fatigue in PBGA assemblies. The model was used to simulate a configuration with a large number of warpage affected solder joints. A regression model based on solder restoring/reaction forces during reflow was used to predict the equilibrium configuration of a warped electronic package. Analyzing two PBGA electronic packages, a 72 I/O cavity-up and a 540 I/O cavity-down assembly, the study showed the reliability of the cavity-down assembly was strongly affected by warpage. Arch and saddle-type warpage changed the shape of the corner solder joint by reducing its height, and thus, fatigue life considerably. The study inferred a bowl-shaped warpage would increase the life of the corner joint beyond that of the no-warpage model because the joint's height would be increased.

Tower, et al., (1999) developed a model to predict yield of flip-chip solder assemblies during solder reflow by considering mean and standard deviation of volume distribution, the assembly warpage, the die size, and the number of input/outputs. Again, a regression model based on solder restoring/reaction forces during reflow was used to predict the equilibrium configuration of a warped electronic package. The model showed a strong correlation between warpage and assembly yield, as warpage increased, yield decreased.

The above-cited studies have ignored the pad rotation that would naturally result from warped electronic packages. Renken and Subbarayan (2000) have shown that a 5° pad rotation could nearly halve the standoff height in area-array solder joints due to the resulting nonsymmetric distribution of droplet volume. Thus, the

inclusion of pad rotation in the present study is believed to have important consequences for the solder joint reliability and the belief that warpage could lead to non-intuitive failures in joints other than the usual "corner joint" at the die edge.

1.4 Summary of Contributions and Thesis Outline

1.4.1 Contributions

The major contributions of thesis can be broken into three areas:

1. An implementation procedure for the analysis of electronic packages based on the decomposition methodology enabling one to determine the equilibrium configuration of electronic packages with significant computational efficiency at a reasonable accuracy.
2. Development of a model and an accompanying computer code for studying the effect of printed circuit board (PCB)/package warpage and solder volume variation on the final equilibrium configuration of area-array packages during solder reflow.
4. Development of a methodology for the analysis of electronic packages with warped solder joints based on the decomposition procedure enabling one to carryout a systematic study of the reliability implications of warpage in electronic packages.

1.4.2 Thesis Outline

In Chapter 2 we introduce the decomposition procedure for the analysis of electronic packages and the code developed utilizing this procedure to analyze electronic packages. The chapter concludes with the developed procedure

demonstrated on two- and three-dimensional hypothetical and "real-world" electronic packages with non-warped solder joints.

In Chapter 3 we describe a model and a computer code for studying the effect of printed circuit board (PCB)/package warpage and solder volume variation on the final equilibrium configuration of area-array packages during solder reflow process. The chapter concludes with the developed procedure demonstrated on hypothetical electronic packages with warped solder joints.

In Chapter 4 we demonstrate the decomposition procedure for analyzing electronic packages with warped solder joints. We then demonstrate the procedure on a three-dimensional hypothetical area-array electronic package. We conclude the chapter with a discussion on the reliability impact of electronic packages with warped solder joints and the consequences of pad rotation/tilt on solder joint reliability.

Chapter 5 concludes the thesis by highlighting the novel contributions in the present study and by making recommendations for future work for further continuation of the present study.

Chapter 2

Applications of a Decomposed Analysis Procedure for Area-Array Packages

2.1 Chapter Overview

In this chapter we introduce the decomposition procedure for analysis of electronic packages and the code developed utilizing this procedure to analyze electronic packages. The developed procedure is demonstrated on two- and three-dimensional hypothetical and "real-world" electronic packages with non-warped solder joints.

Finally to illustrate the usefulness, flexibility and strength of this procedure, we review displacement accuracies, computational efficiencies, and superelement energy contributions.

The objectives of this chapter:

- Refine model for solder response through additional basis terms.
- Demonstrate methodology on "real-world" electronic package.
- Provide insight into decomposed approach.
  - Displacement versus relative displacement errors.

- Provide insight into superelement energy contributions to relative displacement errors.

2.2 Introduction

New products are pushing density and speed of electronic packages to the limits. To support this evolution, packaging technologies are moving at a rapid pace. It is believed by the year 2012, complex electronic packages will contain over 5000+ I/Os (SIA, 1997). Analysis techniques must evolve at an even faster pace if quick decisions regarding package reliability are to be made. Numerical techniques such as finite element analysis are commonly used in determination of stresses and strains, and through these the package reliability. However, with decreasing package size, increasing I/O count, and complex package configurations and materials, finite element analysis has become computationally expensive. Analysis of packages can take hours or even days to complete at the present time, owing primarily to the nonlinear behavior of materials.

Deshpande and Subbarayan (1999) developed and demonstrated an efficient technique for the design/analysis of electronic packages. This procedure is inspired by the domain and design decomposition methodologies literature. The former methods largely address the issue of partitioning a large domain (approximated by a finite element mesh) into well-balanced subdomains (submeshes) that can be efficiently solved on a parallel computer (see for example Farhat et al. 1987, 1989). The latter methods aim to divide a large *design* problem (often posed as an optimization problem) into a series of simpler subproblems for solution efficiency (Haftka and Gurdal, 1992). The procedure of Deshpande and Subbarayan (1999) is

among the first for *simultaneous design and domain* decomposition. They demonstrated a speed-up of approximately 350% at an accuracy loss of only 6% on a hypothetical 5x5 area array procedure. Their analysis of the floating point operations demonstrated an unbounded increase in speed-up for larger array sizes.

During the present research, we develop a general implementation scheme for the technique developed by Deshpande and Subbarayan. The developed code addresses a critical need in the electronic industry for quick reliability decisions. One major aspect of the proposed implementation scheme is the parametric representation of the overall problem that allows the system response to be determined by a relatively few unknowns. This is in contrast to the nonlinear finite element analysis schemes that would require an iterative solution to a large number of nodal unknowns. A second major aspect of the implementation scheme is the underlying optimization procedure that iteratively determines the solution to the unknowns for any area array package described in the required manner.

2.3 Methodology

The first step in the present application of the procedure is a partitioning of the package into solder joints, the component, and the circuit board (Figure 2.1). Further, the parameters that describe the package geometry and its deformation are categorized as design variables and analysis variables. The variables that determine the geometry of the package, or the design variables, are: the sizes of the package and the PCB, the pad diameters, the solder volume and the weight of the package borne by solder joint. The analysis variables are typically the displacements determined for a given geometry. These displacements could occur either within

each subsystem (solder joint, PCB, and component) or at the interface between the solder joints and the component as well as between the solder joints and the PCB. These latter displacements occurring at the interface are in some sense more critical since these displacements characterize the interaction between the subsystems joined at the interface (Deshpande and Subbarayan, 1999).

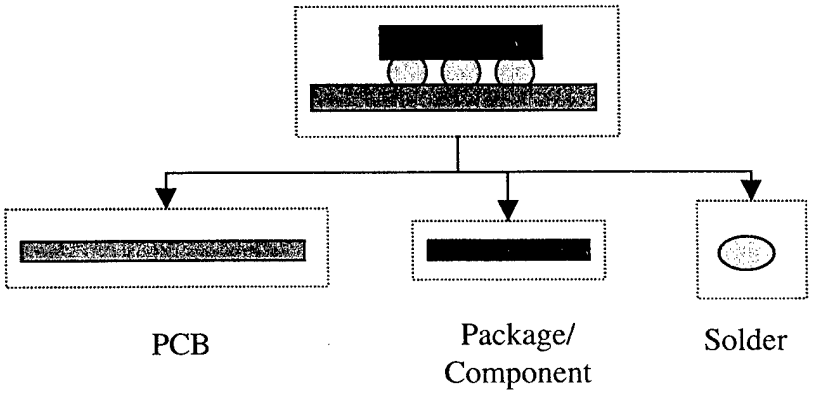

Figure 2.1 Decomposition of electronic packages.

2.3.1 Problem Parameterization

The novelty of the proposed implementation scheme lies in the assumption of displacement fields at solder/component and solder/PCB interfaces and the ability of the code to generate these displacements for any type of array package based on a general code input deck. Each individual solder joint is subjected to relative shear (u–v) and axial (w) displacements. These displacements are due to the *global* mismatch in the values of the coefficients of thermal expansion for the PCB and the component. In addition, the solder joint is subjected to u, v, and w displacements due to the *local* mismatch in thermal expansions between the solder and either the PCB or the component. In general, the u ,v, *and* w displacements across a solder joint due to the combination of global and local mismatches may be non-uniform.

As a first order approximation, we assume this variation to be linear. The differential expansion due to the local mismatch at any point on the interface between the solder joint and the component or PCB is assumed radial in direction with respect to the center of the solder joint. Based on our assumption of linear variations in local displacements, the displacement field across the top and bottom solder joint interfaces can be approximated by eight variables, ξ_0, ξ_1, ξ_2, and ξ_3 at the bottom interface, and γ_0, γ_1, γ_2, and γ_3 at the top interface as shown in Figure 2.2.

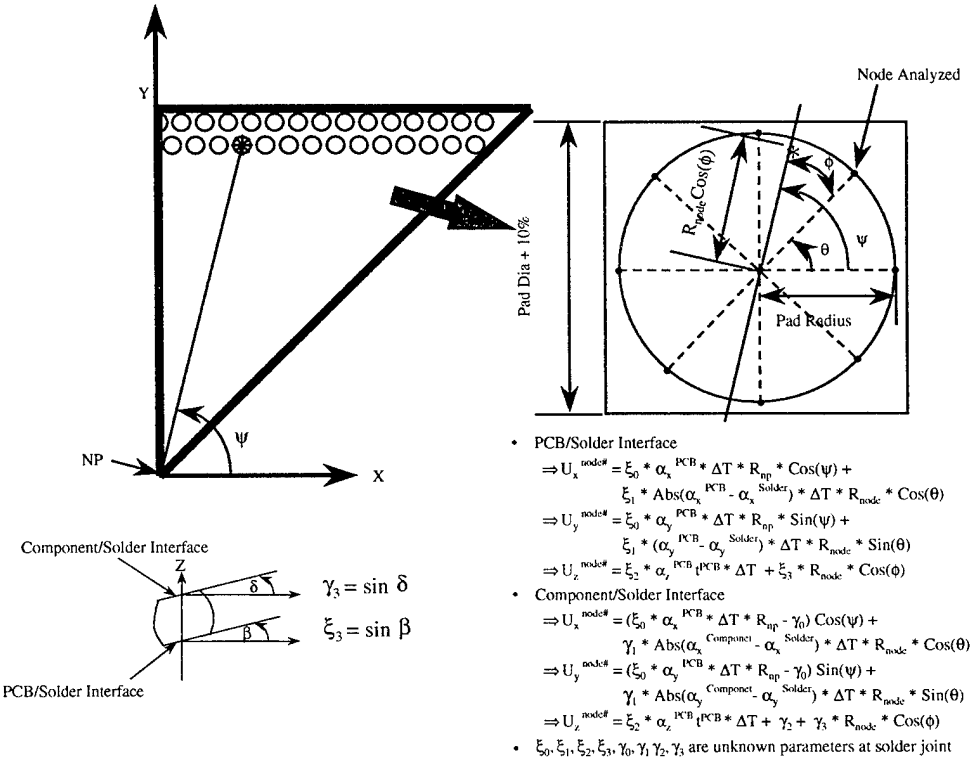

Figure 2.2 Generating displacement fields in the package decomposition.

At the bottom interface, the variable ξ_0 accounts for the *u-v* displacements due to thermal expansion of the PCB, whereas the variable ξ_1 accounts for the *u-v* displacements due to local mismatch at the PCB/solder interface . The actual nodal

u-v displacements are calculated by adding the local and global displacements. The *axial* displacements are assumed to occur along the line connecting the package neutral point to the solder center joint and is represented by a uniform *w* displacement accounted for by variable ξ_2 and a linear variation of slope superimposed on *w* and accounted for by variable ξ_3. The actual nodal *w* displacements are calculated by adding the uniform and the linearly varying components of the *w* displacements. Variable ξ_2 can also account for any bending/warpage of the package due to thermal mismatch.

At the top interface, the variable γ_0 accounts for the *relative shear* displacement of the solder joint due to global thermal mismatch. From this, the actual nodal *u-v* displacements of the component are calculated by subtracting this relative shear displacement from the PCB *u-v* displacement and adding the local *u-v* interfacial displacements, accounted for by variable γ_1. The *relative axial* displacement of the solder joint, γ_2, and linear varying slope imposed on this displacement, γ_3, are added to the axial displacements of the PCB to generate the axial displacements of the component (see Figure 2.2).

The use of the package temperature rise (ΔT), thermal expansion coefficients (α), and geometric entities, such as PCB thickness (t^{PCB}), in calculating the nodal displacements serve to normalize our displacement field variables making the optimization variables scale independent. The approximation of the package behavior using these eight variables greatly reduces the total number of unknowns at each interface, compared to a full nonlinear finite element analysis.

Deshpande and Subbarayan (1999) used only three variables per solder interface (six variables per solder joint) to approximate the *relative* displacement field, u, v and θ, across a solder joint. The displacement u is the relative shear displacement due to global mismatch. The axial displacements are represented by a uniform displacement v and a linear variation with slope θ superimposed on v (see Figure 2.3). In their analysis, the local displacements are assumed constant at each interface.

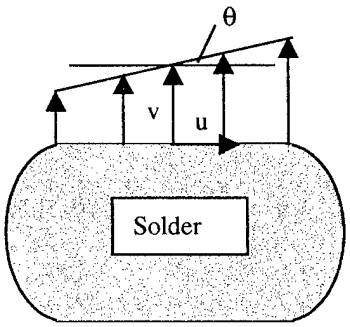

Figure 2.3 Relative displacements in the package decomposition.

In our analysis, the displacements at every interfacial node are captured using four unknown variables, for a total of eight variables per solder joint. These variables are selected based on physical intuition and although there is an increase in the number of optimization variables per solder joint (eight versus six), the present procedure provides a more structured and robust approach to analyzing electronic packages. This approximation is one key factor in increasing the efficiency of the decomposed analysis approach. For a given displacement field, the response of the solder joint was described by the rate at which work is done by the solder joint on the rest of the system and vice versa.

2.3.2 Subsystem Interfacial Work

In area-array packages, the materials used for the construction of PCB and the component can often be approximated as linearly behaving. It should be noted that in a general application of the partitioning methodology, the linear substructure need not be a clearly identifiable subsystem (such as the PCB), and could well be a linearly behaving subdomain of one homogeneous structure. The rate at which energy is stored in these linear substructures (assumed to be discretized by a finite element mesh) for any arbitrary displacement **u** at the retained nodes is given by:

$$\dot{W} = \int_V \sigma_{pq}\dot{\varepsilon}_{pq}dV \approx \mathbf{u}^{\mathrm{T}}\mathbf{K}\dot{\mathbf{u}} \qquad 2.1$$

where σ_{pq} is the stress tensor, $\dot{\varepsilon}_{pq}$ is the rate of strain tensor, and **K** is the reduced stiffness matrix of the substructure or "superelement." The superelements were built using the ABAQUS finite element code in the present study, but most finite element codes allow the calculation of these matrices.

Typically, in any electronic package, the solder joints are nonlinearly behaving subsystems and a detailed nonlinear finite element analysis is necessary to capture the response of these joints. In the developed procedure, the interaction between the solder joints and the rest of the system (PCB or component) at an instant *t* is captured through the rate at which work is done at the solder interface, which is calculated as:

$$\dot{W} = \int_S T_i\dot{u}_i ds \approx \sum_{i=1}^{n} F_i(t)\dot{u}_i(t) \qquad 2.2$$

where n is the total number of nodes; F_i and $\dot{u}_i$ are the forces and velocities respectively, at node i.

2.3.3 Coordinating Subsystems Towards System-level Solution

For the overall energy balance of the system, the three subsystems mentioned earlier must each satisfy the equations governing balance of mechanical energy, as must the package as a whole. Ignoring the rate of kinetic energy enables one to define the equilibrium configuration of the system. The error introduced due to the partitioning of the package can be broadly divided into two categories: those that accumulate at the interface between two subsystems due to incorrectly imposed displacements/tractions at the interface, and those that occur during the solution of the energy balance equation by the finite element method. Since the latter error is unavoidable even when an analysis is carried out without any decomposition, the former error occurring at interfaces is the one that is caused by the decomposition process. Deshpande and Subbarayan (1999) derived a relationship for this error for a general nonlinear system loaded over a step lasting a time Δt as:

$$E = \sum_{k}^{K} \int_{t}^{t+\Delta t} \left(\dot{W}_p + \dot{W}_q \right) dt \qquad 2.3$$

where $\dot{W}$ is the rate of external work, subscripts p and q refer to the two subsystems that share the interface k, and K is the total number of new interfaces introduced due to the partitioning process. K will in general equal one less than the total number of subsystems. If the tractions and displacements at the interface are perfectly matched at every point, and if the displacement field at the interface was exact, then the integrand in Equation 2.3 is zero at every instant. However, approximations in the interfacial displacement field due to the parameterization discussed earlier, or due to

a mismatched mesh (leading to mismatched displacement fields on the two surfaces forming the interface) will cause the integrand to be non-zero.

In the methodology developed, the decomposed solution is obtained by minimizing the accumulated error of Equation 2.3. Thus for a load step over time t, the error to be minimized becomes:

$$\begin{aligned} E &= W_{comp} + W_{sldr/comp} + W_{PCB} + W_{sldr/PCB} \\ &\approx \frac{1}{2}\mathbf{u}_c^{\mathrm{T}}\mathbf{K}_c\mathbf{u}_c - \mathbf{f}_{th_c}\mathbf{u}_c + \sum_0^t \sum_{i=1}^n F_{c_i}\Delta u_{c_i} \\ &+ \frac{1}{2}\mathbf{u}_p^{\mathrm{T}}\mathbf{K}_p\mathbf{u}_p - \mathbf{f}_{th_p}\mathbf{u}_p + \sum_0^t \sum_{i=1}^n F_{p_i}\Delta u_{p_i} \end{aligned} \qquad 2.4$$

Subscript c refers to the component and subscript p refers to the PCB (Deshpande and Subbarayan, 1999). By choosing an incrementally small time step t, the time-dependent response can also be accurately captured in an incremental manner, analogous to the iterative schemes of nonlinear finite element analysis.

The forces acting on any node in the package are the sum of thermal forces and mechanical forces:

$$\mathbf{f} = \mathbf{f}_{th} + \mathbf{f}_R \qquad 2.5$$

where the subscripts th and R refer to the thermal forces and mechanical forces respectively. The thermal forces are the forces developed at the retained nodes of superelements due to thermal strain. The forces $\mathbf{f}_R$ are the result of externally applied tractions at the retained nodes. The ABAQUS finite element code outputs the force vector $\mathbf{f}_{th}$ during the process of building the superelements. Since thermal strains by definition do not cause a mechanical stress, the contribution of the thermal forces is subtracted from the stored energy in Equation 2.4.

If solder joints are assumed to behave linearly (for a preliminary analysis), then the error to be minimized becomes the same as the total potential energy of the system:

$$\begin{aligned} E &= W_{comp} + W_{PCB} + W_{cp_i} \\ &\approx \frac{1}{2}\mathbf{u}_c^{\mathrm{T}}\mathbf{K}_c\mathbf{u}_c - \mathbf{f}_{th_c}\mathbf{u}_c + \frac{1}{2}\mathbf{u}_p^{\mathrm{T}}\mathbf{K}_p\mathbf{u}_p \\ &\quad -\mathbf{f}_{th_p}\mathbf{u}_p + \frac{1}{2}\mathbf{u}_{cp_i}^{\mathrm{T}}\mathbf{K}_s\mathbf{u}_{cp_i} - \mathbf{f}_{th_s}\mathbf{u}_{cp_i} \end{aligned} \qquad 2.6$$

As stated earlier, the component and PCB behavior can be approximated as being linear. In Equation 2.6, subscript s refers to the solder and subscript cp_i of the fifth and sixth terms refers to the solder interface with component and PCB and, these terms replace the third and sixth terms of Equation 2.4. Vector $\mathbf{u_{cp}}$ is an augmented vector comprising of vectors $\mathbf{u_c}$ and $\mathbf{u_p}$. Thus, for assumed displacement vectors $\mathbf{u_c}$ and $\mathbf{u_p}$ the error defined by Equation 2.6 can be calculated, and the process iterated until the displacement vectors that yield the minimum error are obtained.

The equilibrium state of the system as a whole is approximated by minimizing the error function of Equation 2.4 in the present procedure. The evaluation of the terms in Equation 2.6 is very inexpensive and straightforward once the superelement stiffness matrix is calculated. The computational expense in evaluation of Equation 2.4 is due to the need for evaluation of the work defined in Equation 2.2 for the nonlinearly behaving solder alloy.

2.3.4 Numerical Simulations to Approximate Solder Joint Response

Following the Simultaneous Analysis and Design (SAND) idea applied by Deshpande et al. (1998), a statistically designed set of simulations are carried out

next to capture the nonlinear response of the solder joints to changes in design and analysis related parameters. For this modeled response to be valid for the widest possible choice of future and present packages, careful thought must be given to the input parameters and their ranges. These issues are described in detail by Deshpande et al. (1998), and only the points of major difference with the prior research are described in the brief outline below.

In the present study, a range of 0.0-2.0 microns for the relative shear displacement (u) and a range of 0.5-2.0 microns for the relative axial displacement (v) were chosen. The linear variation of the axial displacement represented by the angle θ was assumed to have a range of -1° to 1°. These ranges were based on Moiré experiments on several 225 I/O PBGA packages that indicated a peak relative shear displacement of approximately 1.8 microns, for a temperature change of –80 °C (Zhang et.al, 1998). In addition, work due to local mismatch at each interface was captured by varying the top and bottom expansion, α_1 and α_2, coefficients from 7 to 21 ppm/°C. A fractional factorial designed "experiment" (Montgomery, 1997) based on the five levels of these variables, as shown in Table 2.1, was used to capture the response of the solder joint.

Table 2.1 The fractional factorial designed experiment used to build regression model for solder work.

Run	u (μm)	v (μm)	θ (radians)	α1 (ppm/°C)	α2 (ppm/°C)	Work (N-μm)
1	2	2	0.017455	21	21	25.50
2	2	2	0	21	14	8.32
3	2	2	-0.017455	21	7	34.58
4	2	1.25	0.017455	14	21	24.01
5	2	1.25	0	14	14	4.92
6	2	1.25	-0.017455	14	7	33.20
7	2	0.5	0.017455	7	21	24.33
8	2	0.5	0	7	14	5.53
9	2	0.5	-0.017455	7	7	33.65
10	1	2	0.017455	14	14	26.88
11	1	2	0	14	14	6.31
12	1	2	-0.017455	14	14	31.38
13	1	1.25	0.017455	14	14	25.50
14	1	1.25	0	14	14	2.30
15	1	1.25	-0.017455	14	14	30.00
16	1	0.5	0.017455	14	14	25.73
17	1	0.5	0	14	14	2.71
18	1	0.5	-0.017455	14	14	30.25
19	0	2	0.017455	21	21	28.93
20	0	2	0	21	14	5.69
21	0	2	-0.017455	21	7	29.13
22	0	1.25	0.017455	14	21	27.40
23	0	1.25	0	14	14	1.11
24	0	1.25	-0.017455	14	7	27.75
25	0	0.5	0.017455	7	21	27.74
26	0	0.5	0	7	14	2.07
27	0	0.5	-0.017455	7	7	28.22

A non-linear elastic-plastic analysis was performed on each of the twenty-seven settings in the designed experiment using the integrated solder shape/life prediction method developed by Subbarayan (1996). A typical finite element model of the solder joint generated by using this methodology is shown in Figure 2.4. For given values of the design variables, the program developed by Subbarayan predicts the shape of the solder joints and the shape is then automatically converted into a 3-D finite element mesh, which is analyzed using the ABAQUS finite element code.

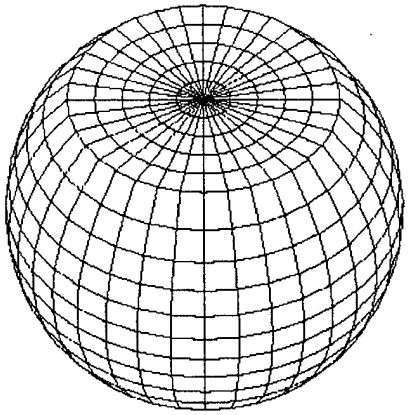

Figure 2.4 A typical finite element model of the solder joint.

Linear regression models were built to relate the work quantities defined in Equation 2.4 with the five input parameters. These regression models represent a stand-alone module for solder joints. Even though the five inputs to this module are analysis-related parameters (u and v displacements, θ, α_1 *and* α_2), it is quite simple to add design-related variables such as the solder volume and/or solder pad diameters as additional variables to this module. Such a module can be used in the design and analysis of packages with widely different geometries as discussed by Deshpande et.al. (1998). In general, the regression models are possible only under monotonic loading conditions since the stress-strain relation and therefore the inelastic dissipation is non-unique (or history dependent) under reversed loading conditions. Thus, while the developed methodology is general and applicable to reversed loading conditions, the regression model's validity is limited to monotonic loading conditions.

2.3.5 Code and Code Input Deck

The code developed must be general enough to solve many types of electronic packages. A major aspect of the implementation scheme is the underlying optimization procedure that iteratively determines the solution to the unknowns for any area array package. Our code incorporates the non-linear optimization code NLPQL (Schittkowski, 1985). This code iteratively improved the variables until the optimum point was reached. The NLPQL routine finds the minimum or maximum of a nonlinear function of n optimization variables subject to nonlinear or linear constraints using a Sequential Quadratic Programming (SQP) method. The gradients were calculated at each iteration by forward differences. However, as the size of the packages increase, so will the number of optimization variables and number of function evaluations. Use of numerical gradients subroutines with NLPQL require $(n+1)$ function evaluations at each iteration. For example, a 225 I/O area-array package with 36 solder joints at 1/8 scale (288 optimization parameters) would require 289 function evaluations at each iteration. This can be computational expensive with CPU times approaching or exceeding that of a full three-dimensional non-linear finite element analysis. In implementing our scheme, we developed an analytical gradient subroutine for the package's linear substructures. This reduced the number of function and gradient evaluations to one each for a total of two evaluations per iteration, greatly decreasing CPU times. The gradient of the error function (Equation 2.4) is calculated in the code as:

$$\frac{dE}{dx} = \mathbf{K}_c \mathbf{u}_c \frac{\mathbf{du}_c}{\mathbf{dx}} - \mathbf{f}_{th}^c \frac{\mathbf{du}_c}{\mathbf{dx}} + \mathbf{K}_p \mathbf{u}_p \frac{\mathbf{du}_p}{\mathbf{dx}} - \mathbf{f}_{th}^p \frac{\mathbf{du}_p}{\mathbf{dx}} + \frac{\mathbf{d}W}{\mathbf{du}} \frac{\mathbf{du}_W}{\mathbf{dx}} \qquad 2.7$$

where W is the regression model for the accumulated work done by the solder joint.

A typical input deck needed to successfully run the code is shown in Figure 2.5. With this input deck, the code generates the displacement field at each interface by first matching the retained interfacial nodes with the appropriate solder joint center node. The program then proceeds to calculate the distance from the package neutral point to each joint center, R_{np}, and the distance from the matching nodal points to the joint center, R_{node}. By determining where the joint centers lie at solder/component interface or solder/PCB interface, the code generates the displacement fields. Figure 2.6 illustrates the flow of control within the developed procedure.

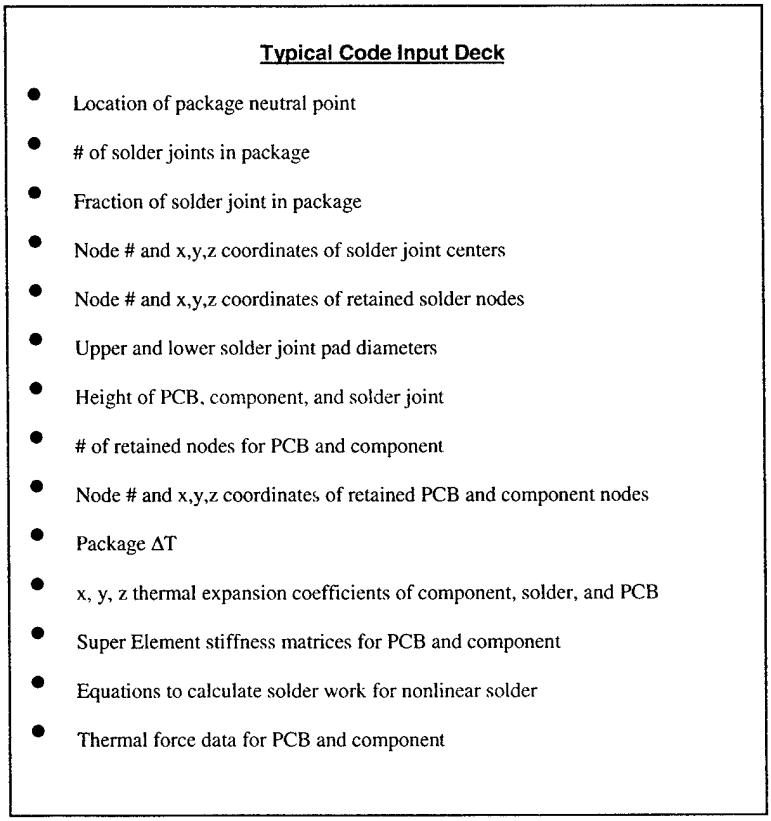

Figure 2.5 Typical code input deck.

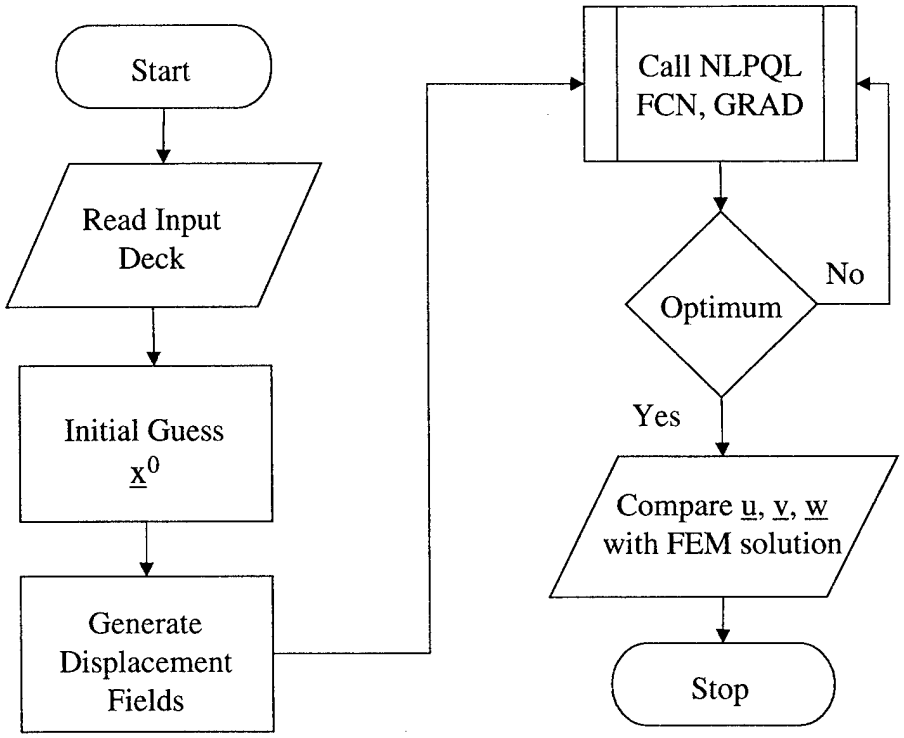

Figure 2.6 Flow control in the program.

2.3.6 Solving for the Displacements

The decomposition methodology described earlier was applied systematically to two 2-D electronic packages, Deshpande and Subbarayan's 3-D 5x5 hypothetical electronic package, and a 225 I/O PBGA electronic package as described below. For the purposes of verification of the code, the solder material was initially assumed to behave linearly. This is not a limitation of the code, but an assumption that enabled quick testing of the developed code. The finite element models of the 2-D packages are shown in Figure 2.7. The first package has only one solder joint (2 interfaces with 8 unknown variables) and the second package has 3 solder joints (6 interfaces with 24 unknown variables). The full three-dimensional finite element model of the

5x5 hypothetical area-array package is shown in Figure 2.8. The cross-section of this package is shown in Figure 2.9. Because of symmetry, only one-eighth of the package was modeled which had 6 solder joints (12 interfaces with 48 unknown variables). A full three-dimensional finite element model of the 225 I/O PBGA package was also built and is shown in Figure 2.10. The cross-section of this package is shown in Figure 2.11. A one-eighth symmetry model of the 225 I/O package has 36 solder joints (72 interfaces with 288 unknown variables).

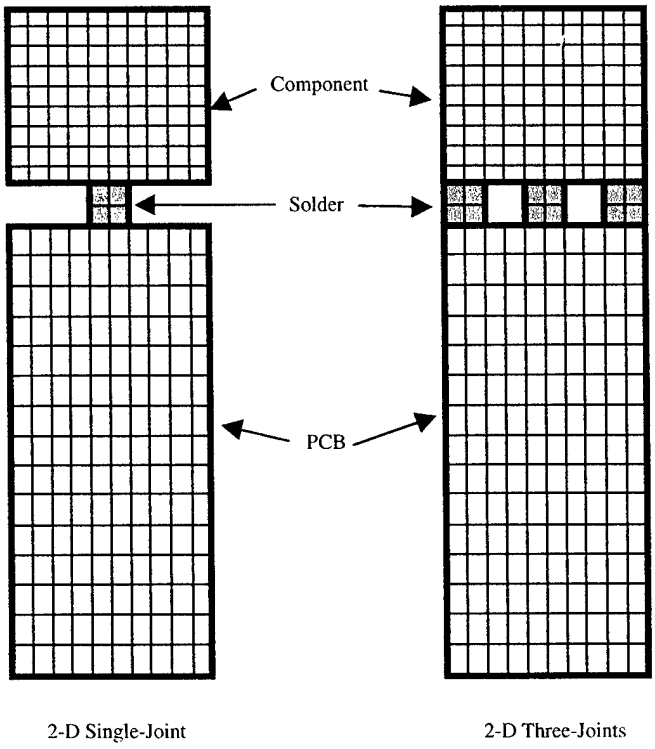

Figure 2.7 Finite element models of hypothetical 2-D electronic packages.

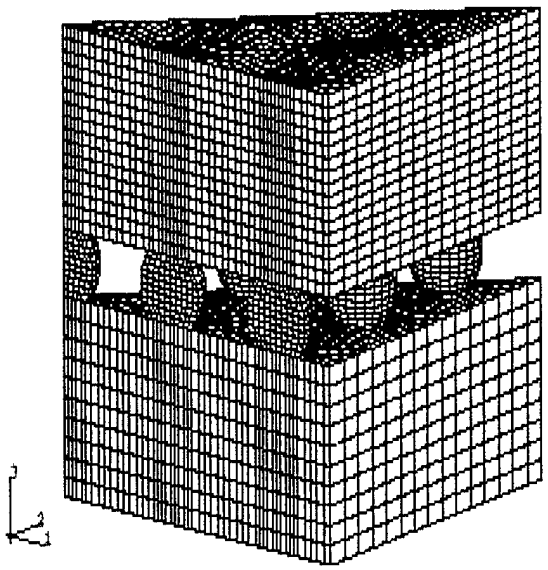

Figure 2.8 The 3-D FE model of the 5x5 package.

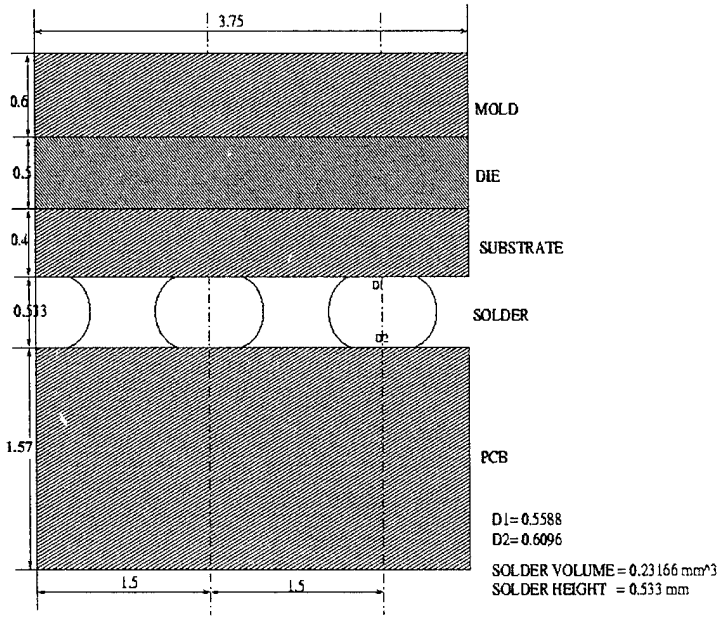

Figure 2.9 The cross-section of the hypothetical 5x5 model.

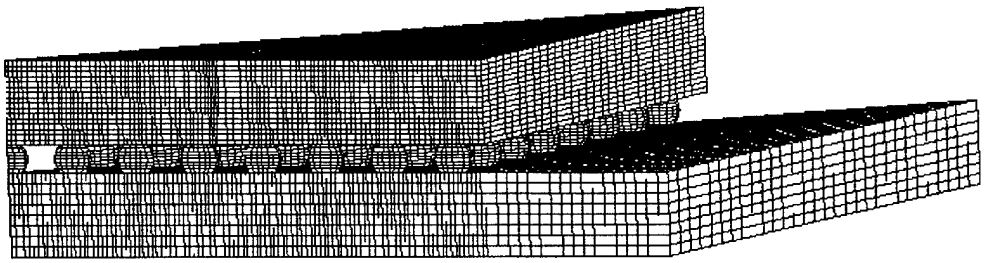

Figure 2.10 The 3-D FE model of the 225 I/O PBGA electronic package.

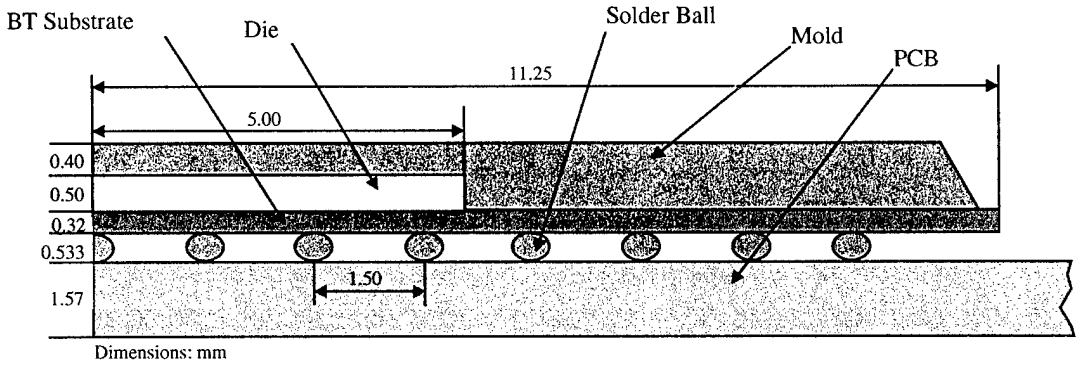

Figure 2.11 Cross-section of the 225 I/O PBGA electronic package.

The material properties for the 2-D models are shown in Table 2.2. The material properties for the 3-D models were chosen to be the same as that given in Deshpande et.al. (1998) and are shown in Table 2.3. The 2-D models were subjected to a uniform temperature rise of 100°C from the initial temperature of 0°C and the 3-D models were subjected to an 80°C temperature rise from the same initial temperature.

Table 2.2 Material properties used in 2-D electronic packages.

Material	Temperature (°C)	Modulus E (GPa)	Poisson's Ratio	CTE (In-Plane)	CTE (Out-of-Plane)
PCB (FR-4)	20	15.5	0.20	1.47E-05	5.12E-05
Component (Silicon)	20	131	0.28	2.60E-06	2.60E-06
Solder (63Sn37Pb)	0	32	0.35	2.10E-05	2.10E-05
	20	30			
	50	27			
	100	22			

Table 2.3 Material properties used in 3-D electronic packages.

Solder (63Sn37Pb)					
E (GPA)	Poisson's Ration	Temperature °K	Yield Stress (GPA)	Plastic Strain	Temperature °K
34.055	0.3	273	0.0138	0	273
33.329	0.3	278	0.0276	7.30E-04	273
32.603	0.3	283	0.0414	7.02E-03	273
31.877	0.3	288	0.0552	3.49E-02	273
31.151	0.3	293	0.0689	1.21E-01	273
30.425	0.3	298	0.0827	3.36E-01	273
29.699	0.3	303	0.0965	7.93E-01	273
28.973	0.3	308	0.1100	1.67E+00	273
28.247	0.3	313	0.1240	3.22E+00	273
27.522	0.3	318	0.1380	5.80E+00	273
26.796	0.3	323	0.0138	0	373
26.07	0.3	328	0.0276	1.62E-02	373
25.344	0.3	333	0.0414	1.56E-01	373
24.618	0.3	338	0.0552	7.76E-01	373
23.892	0.3	343	0.0689	2.70E+00	373
23.166	0.3	348	0.0827	7.46E+00	373
22.44	0.3	353	0.0965	1.76E+01	373
21.714	0.3	358	0.1100	3.71E+01	373
20.988	0.3	363	0.1240	7.16E+01	373
20.262	0.3	368	0.1380	1.29E+02	373
19.536	0.3	373			
CTE = 21.0E-6					

BT Substrate	PCB	Die	Over Mold
E (GPA)	E (GPA)	E (GPA)	E (GPA)
19.0	18.2	130.0	15.5
Poisson's Ratio	Poisson's Ratio	Poisson's Ratio	Poisson's Ratio
0.2	0.19	0.28	0.25
CTE	CTE	CTE	CTE
1.50E-05	1.60E-05	2.62E-06	1.50E-05

The displacements obtained with decomposed analysis procedure were compared with those obtained using non-decomposed, full finite element models. The analysis was carried out using the ABAQUS finite element code (HKS, 1997). In addition, the assumption of linear elastic behavior in our preliminary analyses, gave us the opportunity to test the non-linear optimization code NLPQL by *assuming all nodal displacements as unknown variables* and comparing the results with the full finite element analysis. In this case, the present procedure reduces to that of the classical substructuring approach of finite elements, only the solution is obtained using an iterative approach as opposed to using matrix factorization methods. The error between the iterative and non-iterative solutions in these cases was negligible.

2.3.7 Error Measures

Finally, a discussion of the error measures used to evaluate the accuracy of the decomposed analysis procedure is in order. In keeping with the parameterization scheme discussed earlier and illustrated in Figure 2.2, the errors in displacements may be divided into two kinds. The first kind is the error in displacement at any interfacial node, expressed in a suitable non-dimensional form. This is referred to as the displacement error or simply the error in the present paper. Mathematically, the chosen error is Euclidean in form and is defined as:

$$Error_M = \frac{\left(\sum_{i=1}^{N}(y_i - \hat{y}_i)^2\right)^{1/2}}{\left(\sum_{i=1}^{N}(y_i)^2\right)^{1/2}} \qquad 2.8$$

$$AverageError = \frac{1}{M}\sum_{i=1}^{M} Error_M \qquad 2.9$$

where M is the total number of displacement DOFs for component and PCB, N is the total number of solder nodes, y_i is the displacement predicted by the full FE simulation (the reference for evaluating the accuracy of the decomposed procedure) at the interface, and $\hat{y}_i$ is the solution from the decomposed analysis at the exact same location.

The second kind of error is that in the *difference* between displacements at two points. This is useful in calculating the relative shear and axial displacements of the solder joints, which in turn are important for predicting the fatigue life of the joint under cyclic loading. This error is denoted as the relative error and its average value is mathematically defined as:

$$Average\,\mathrm{Re}\,lativeError = \frac{\left(\sum_{i=1}^{J}(y^{i}_{relative} - \hat{y}^{i}_{relative})^{2}\right)^{1/2}}{\left(\sum_{i=1}^{J}(y^{i}_{relative})^{2}\right)^{1/2}} \qquad 2.10$$

where J is the total number of solder joints, $y^{i}_{relative}$ is the difference in displacements between two nodes in the full FE model, and $\hat{y}^{i}_{relative}$ is the same difference calculated using the decomposed analysis. Since the relative error measures the error in displacement difference, it represents a higher order error compared to the displacement error.

2.4 Results and Discussion

Tables 2.4 lists the results of the analysis using the decomposed solution with displacement fields as compared to the finite element solution. The average displacement error is 0.74% for the single-joint 2-D model and 5.0% for the three-joint 2-D model. The average displacement error for the 3-D 5x5 area-array model with linear solder joints was 6.04% while the average relative shear and axial displacement errors were 6.65% and 6.03% respectively. The 3-D 5x5 area-array model with nonlinear solder joints had an average displacement error of 4.98% while the relative shear and axial errors were 9.00% and 16.43% respectively. This illustrates the difficulty in achieving small relative errors. Lastly, the 225 I/O PBGA model had an average displacement error of 5.46%, while the relative shear and axial errors of 41.93% and 14.42% respectively. Decomposed and the full FE analysis displacement plots for the 5x5 and 225 I/O arrays are shown in Figures 2.12 and 2.13.

Table 2.4 Displacement errors at component and PWB interfaces.

Decomposed Model	Displacement Error (%)			Relative Displacement Error (%)		R^2		
	u	*v*	*w*	*shear*	*axial*	*u*	*v*	*w*
2-D Single Joint - Component	1.78	0.00		2.26	1.34	0.9997	0.9998	
2-D Single Joint - PWB	1.11	0.06				0.9997	0.9998	
2-D Three Joint - Component	11.33	0.19		9.31	5.01	0.9855	0.9998	
2-D Three Joint - PWB	8.28	0.29				0.9264	0.9998	
5x5 Array w/ Linear Solder - Component	5.74	6.55	6.27	6.65	6.03	0.9815	0.9913	0.8135
5x5 Array w/ Linear Solder - PWB	4.81	4.51	8.36			0.9837	0.9949	0.8650
5x5 Array w/ Nonlinear Solder -Component	7.63	5.60	5.42	9.00	16.43	0.9626	0.9929	0.5263
5x5 Array w/ Nonlinear Solder - PWB	1.95	2.12	7.12			0.9974	0.9989	0.3981
		Average	**4.98**					
225 PBGA w/ Nonlinear Solder- Component	2.29	3.71	8.75	41.93	14.42	0.9970	0.9964	0.8694
225 PBGA w/ Nonlinear Solder - PWB	4.48	3.96	9.58			0.9814	0.9936	0.8612
		Average	**5.46**					

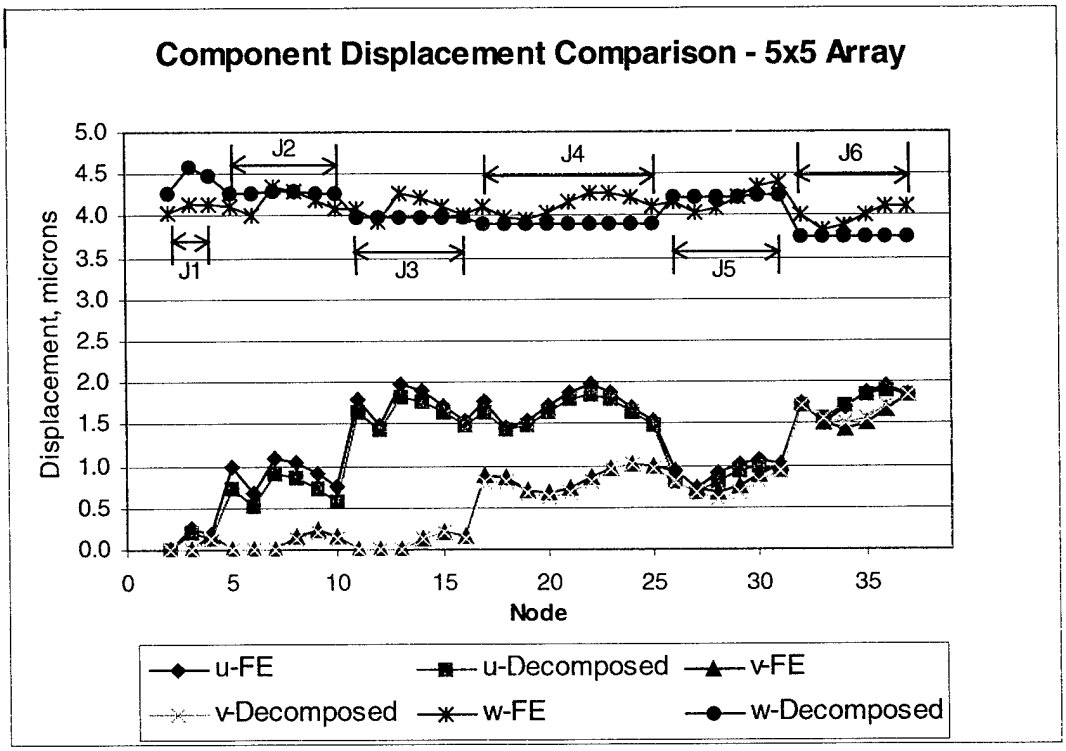

Figure 2.12 Component displacement comparison for 5x5 area-array model depicting solder joints 1-6 (J1 – J6).

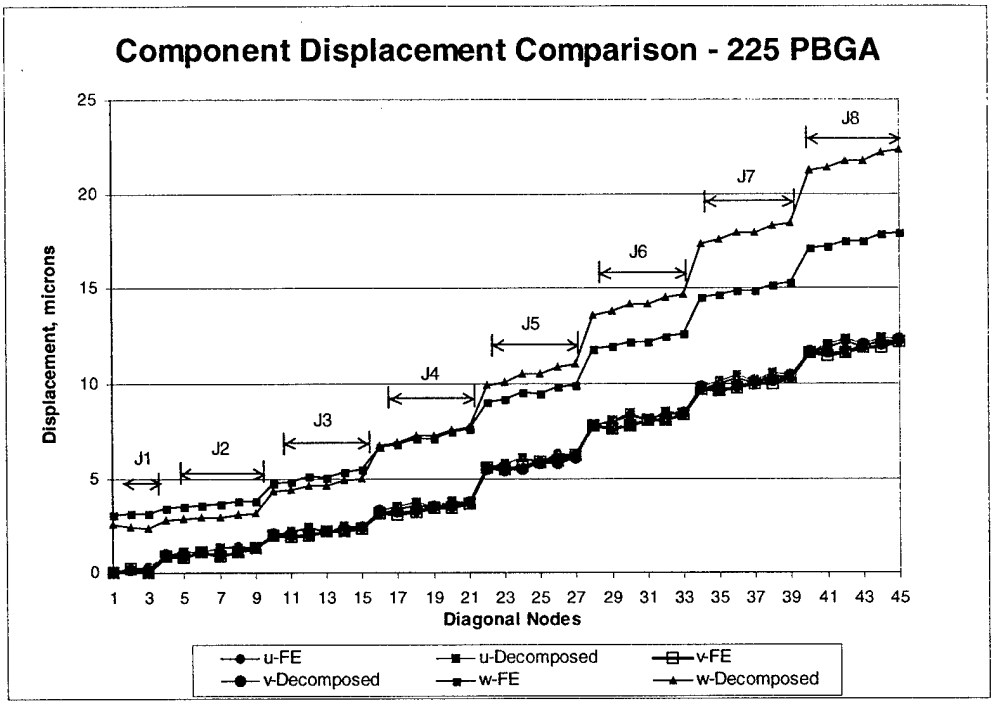

Figure 2.13 Component displacement comparison for 225 I/O PBGA Package depicting diagonal solder joints 1-8 (J1 – J8).

For the 2-D models, the major effort in creating a new code input deck was the generation of new superelement matrices for the component and PCB. This merely involved modifying the ABAQUS input file to retain the additional nodes, which took a few minutes. Each solder joint, although an individual subsystem, is a "repeated" structure within the electronic package, thus the same superelement matrix can be used for each solder joint. Exploiting the nature of these repeated structures enables a considerable computational advantage. Therefore we see by simply changing the code input deck, we are able to carry out a second analysis.

As for the 3-D 5x5 package, superelements were already available. The code was easily modified to handle three-dimensional packages, as was the code input deck. For the case with the nonlinearly behaving solder, the regression model for the work defined in Equation 2.4 was:

$$W = 3.05369 + 1.73768\,u + 1.73116\,v - 2.25479\,\theta - 0.09433\,\alpha_1 - 0.13001\,\alpha_2 - 0.13157\,u\,v\text{^}2 - 1.14245\,u\,\theta^2 - 1.12784\,v\,\theta^2 + 0.55165\,u^2 - 2.21197\,u\theta + 1.36305\,v\text{^}2 + 24.235\,\theta^2 \qquad 2.11$$

The regression model for the experiment was accomplished using the commercially available software *DOE KISS* (Design-of-Experiment Keep-It-Simple-Statistically) for Microsoft Excel (Digital Computations, 1997). The factors in the equation are represented by coded variables where the low and high levels of each factor are assigned the values of –1 and +1.

Table 2.5 shows the CPU times for the decomposed and FE analyses. The CPU time required for the 3-D ABAQUS non-linear analysis of the 5x5 hypothetical package was 5846 seconds on a Pentium-II 400 MHz dual processor machine, whereas the decomposed procedure required only 37 seconds of CPU time on the same machine. Including the CPU time for the 27 experiments (3923 seconds) and superelements (4 seconds), a 47% savings in computational effort was achieved through decomposition. However, we note that for additional package constructions using the same solder joint, the CPU time for the 27 experiments is redundant since the regression model is reusable! This illustrates the power of the decomposed analysis approach.

The CPU time required for the 3-D ABAQUS non-linear analysis of the 225 I/O PBGA package was 23782 seconds on a Pentium-II 400 MHz dual processor machine, whereas the decomposed procedure required only 907 seconds of CPU time on the same machine. Including the CPU time for building the superelements (2195 seconds) but ignoring the time required to build the regression model (for

reasons mentioned above), a 667% speedup in computational effort was achieved through decomposition.

Table 2.5 CPU times (seconds).

	5x5 Decomposed Model	225 Decomposed Model
Super Elements	4	2195
Solder DOE	3923	0
Decomposed Analysis w/ FD Gradients	312	N/A
Decomposed Analysis w/ Analytic Gradients	37	907
Total w/ FD Gradients	4239	N/A
Total w/ Analytical Gradients	3964	3102
3-D Finite Element	5846	23782
CPU Savings	47%	667%

There are two main reasons for these computational savings. The first reason is that the 3-D models have a much larger number of nodes and elements necessitated by the need to match the refined solder mesh in the PCB and the component. The full FE model of the 225 I/O PBGA package had over 94000 nodes and over 90000 elements, whereas in the decomposed analysis, the component and PCB superelements were coarsely meshed and together they contained less than 11,000 elements and 12,000 nodes. The second reason is that the problem with many unknown degrees of freedom at the interface has been reduced to only four unknowns by approximating the displacement fields at the interface through the chosen parameterization scheme. Thus, the parameterization represents a set of basis functions for the displacement at the interface, chosen with the benefit of physical intuition.

The main sources of errors in the displacements can come from: statistical errors in the regression model, finite element solution errors in capturing the non-linear solder behavior, and the errors in the ability of the chosen basis functions to

represent the exact displacement field at the interface. The regression model used here had a goodness of fit measured by an R^2 value of higher than 0.99. This suggests that the regression model is unlikely to be a major source of error. To check if material behavior could be a source of error, analysis of the 5x5 area array package was repeated by assuming linear elastic material behavior for solder joints. In this case, since the behavior was linear, a superelement was built for the solder joint and the response of the solder joint was calculated as described by Equation 2.6. Thus closed form equations for work done were available for all the three subsystems and no regression model was necessary. As stated earlier, the average relative shear and axial errors were 6.65% and 6.03% respectively (See Table 2.4). However, the average overall displacement error with linear solder behavior is approximately the same as the average error in displacements with the non-linear solder behavior, around 5.0 – 6.0%. This suggests that an inaccuracy in capturing the non-linear solder material behavior is unlikely to be the major source of error in the displacements and that the major source of error is due to the approximation introduced by representing the interfacial displacements using linearly varying shear and axial displacements.

The 225 I/O PBGA package had comparatively large axial displacement and relative shear displacement errors. Figure 2.14 (reproduced from Zhang et al., 1999) shows the relative shear displacement along the diagonal joints of the 225 I/O PBGA package determined experimentally through moiré interferometry, and compared to axisymmetric, full 3-D finite element, and decomposed models. The large error in the decomposed solution beyond the die region is due to this region's relative contribution to the overall error function of Equation 2.4. In Figure 2.15, the

relative shear displacement errors is overlaid on the error gradient with respect to variable γ_0 which accounts for the *relative shear* displacement of the solder joint due to thermal mismatch. As seen in the figure, the gradients within the die area of the package are larger than the gradients outside of the die area. This can be attributed to the die area being stiffer (die has larger Young's modulus) than the rest of the package. Since the iterative steps of the NLPQL routine depend on the magnitude of the gradients, it is natural that the larger gradients in the die region receive a greater attention. In Figure 2.15, it can be seen that the relative shear displacement errors for the solder joints within the die region of the package are between 10% to 15% while the errors outside of the die area can range from 25% to 85%.

One may attempt to scale the gradients in such a manner that they are all of equal magnitude, but such a step is unnecessary if one is interested in identifying the critical solder joint. This is since, the solder joint with maximum relative displacement is at the die edge (joint number 3 from center) and as Figure 2.14 shows the decomposed relative shear displacement at this joint agrees well with the full 3-D finite element model and experimental data.

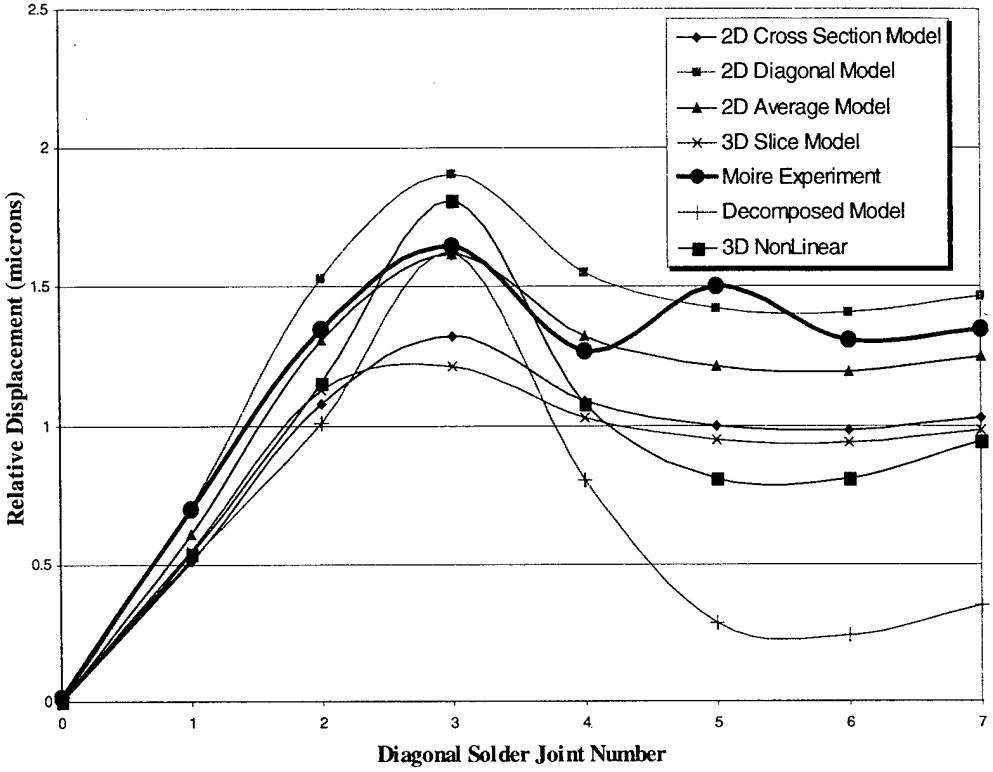

Figure 2.14 Relative shear displacement comparisons (Zhang, et al., 1999).

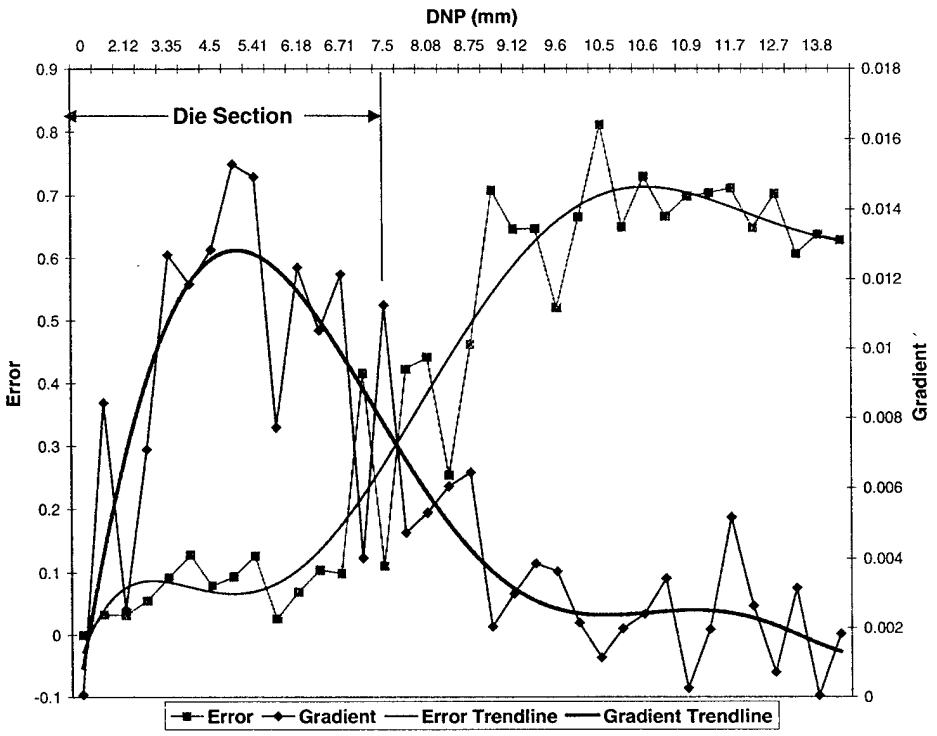

Figure 2.15 225 PBGA shear gradient/relative error plot.

Finally, we found that the use of explicit gradient subroutines decreased the CPU time for the decomposed solution procedure significantly. Analysis of the 5x5 area-array model using both finite difference and analytic gradients showed a 275 second decrease in CPU time from 312 to 37 seconds. For a larger package, such as the 225 I/O PBGA, the decomposed analysis proved not to be practical without the analytical gradients.

2.5 Conclusions

The present study has demonstrated that using the decomposition method and a more structured approach to generating displacement fields, an accurate solution can be obtained with substantial savings in the computational effort. For example, a 667% speedup was achieved using the decomposed analysis procedure on the 225

I/O PBGA package compared to a three-dimensional nonlinear finite element analysis. Deshpande and Subbarayan (1999) showed the methodology to be scalable to arbitrary package sizes with potentially orders of magnitude savings in computational effort. The methodology can be applied to a wide range of package constructions by just providing a new code input deck. Currently research is underway to develop methods to further reduce the relative error.

Chapter 3

A Model For Assessing The Shape Of Solder Joints In The Presence Of Board Warpage And Volume Variation In Area-Array Packages

3.1 Chapter Overview

In this chapter we introduce novel methodology studying the effect of printed circuit board (PCB) warpage and solder volume variation on the final equilibrium configuration on area-array packages. The developed procedure is demonstrated on a three-dimensional hypothetical electronic package.

The objectives of this chapter:

- Apply homogeneous transformation theory to predict equilibrium configuration of electronic packages.
  - Use rigid rotations of package.
  - Predict equilibrium in presence of arbitrary warpage.
- Validate methodology.

3.2 Introduction

Area-array packages in general are increasingly popular choices in the drive towards cost reduction and miniaturization. They offer enormous area reductions in

comparison to quad flat packages (QFPs) and increasing potential to do so without adding to system-level costs. As with any type of electronic package, reliability is one of the major concerns, with low cycle fatigue of solder joints being one of the most common failure mechanisms. Numerical techniques such as finite element analysis are commonly used to determine package reliability. These reliability assessment techniques normally consist of three basic steps to calculate (Subbarayan, et al., 1999)

1. solder joint shapes,
2. thermal stress/strain distribution in the most susceptible joint after solidification and during thermal cycling, and
3. fatigue lives of the most susceptible or any other selected solder joints.

The ultimate goal of the present research is to understand and systematically study the reliability implications of component and circuit board warpage and solder volume variations since it is believed that warpage could lead to non-intuitive failures in joints other than the usual "corner joint" at the die edge. However, this chapter deals with the first step mentioned above. The end result is a tool to accurately characterize the shapes of solder joints affected by design specifications, e.g., solder height, volume, circular pad diameter, weight of the package borne by solder joint, and manufacturing variations, e.g. warpage.

Solder joint shape resulting from warped circuit boards have not received much attention in the literature. Chan, et al., (1997) and Tower, et al., (1999) appear to be the only studies of this nature. Chan, et al., established a reliability model to study thermal fatigue in plastic ball grid array assemblies. The model was used to

simulate a configuration with a large number of warpage affected solder joints. Tower, et al., developed a model to predict yield of flip-chip solder assemblies by considering mean and standard deviation of volume distribution, the assembly warpage, the die size, and the number of input/outputs. These studies, however, ignored the pad rotation that would naturally result from warped circuit boards. Renken and Subbarayan (2000) have shown that a 5^{o} pad rotation could nearly halve the standoff height in area-array solder joints due to the resulting nonsymmetric distribution of droplet volume (See Figure 3.1). Thus, the inclusion of pad rotation in the present study is believed to have important consequences for the solder joint reliability. The developed methodology is general in nature and is demonstrated on a hypothetical 3x3 area-array package shown in Figure 3.2. The size of the package is 1.2 cm x 1.2 cm, and the diameter of the solder pads on the package and PCB is 0.375 mm. The number of I/O's is 9 with a 5.0 mm pitch.

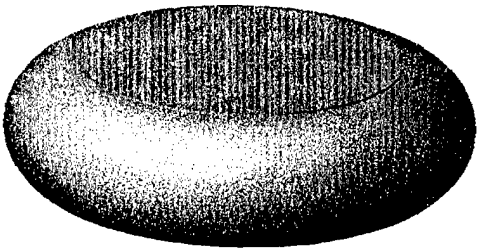

Height before tilt: 57.84 microns

Height after tilt: 32.2 microns

Figure 3.1 Warped solder joint.

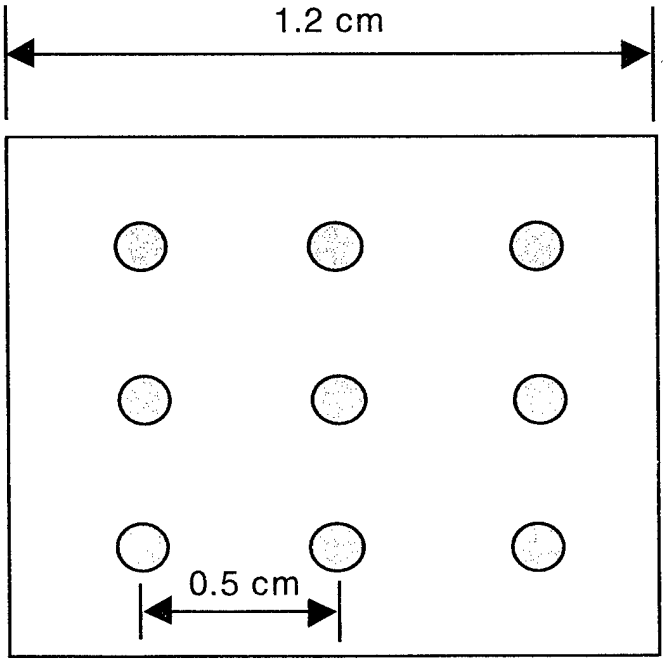

Figure 3. 2 Hypothetical 3x3 array.

3.3 Methodology

3.3.1 Model Overview

The model developed in the present study was based on the following assumptions.

1. Circular pads of the same size were used on both the package and PCB.
2. The assembly warpage value and subsequent warpage shape, e.g., arch, bowl, or saddle, of the package and PCB are known (See Figure 3.3).
3. Solder mean volume and standard deviation, based on a normal distribution, can be given as inputs.

The static equilibrium of the system is achieved when the forces and moments on the package are balanced. These forces and moments result from the restoring forces and moments of the individual solder joints.

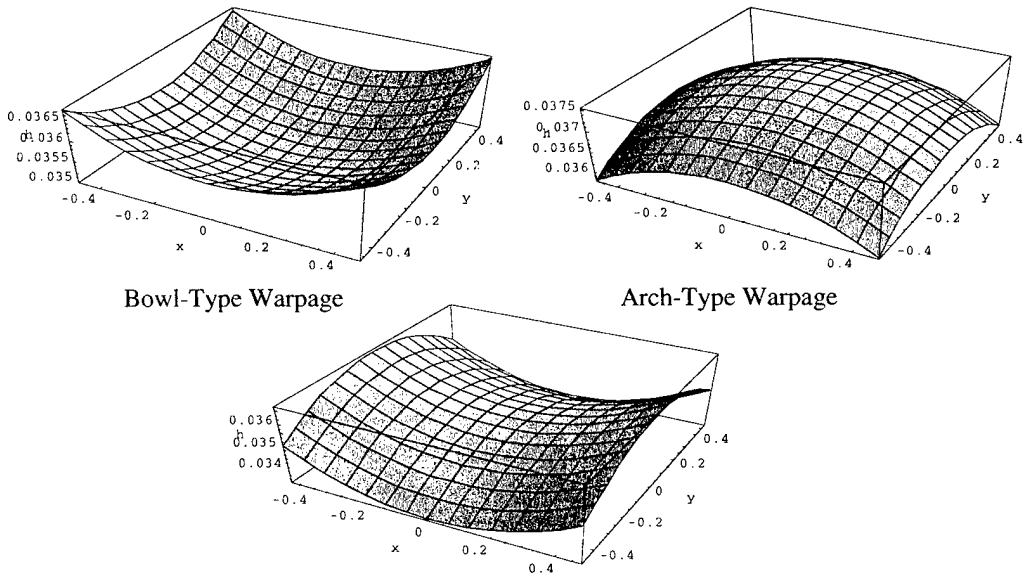

Figure 3.3 Types of warpage.

As illustrated in Figure 3.4, on a single joint, the restoring shear and normal forces together with the restoring moment balance the applied load, F_a, in the z direction and the applied moment, M_a, about the x-axis. However, the package rotation/translation together with the PCB warpage will orient the top and bottom pads in a configuration that is quite different from the reference configuration shown in Figure 3.4. Thus, the package transformation and the PCB warpage have to be mathematically described and their effects transformed to the reference configuration so the restoring forces and moments can be calculated. In the following sections, the warpage, the package motion, the calculation of restoring forces and the transformation of warped configuration to the reference one are described in detail.

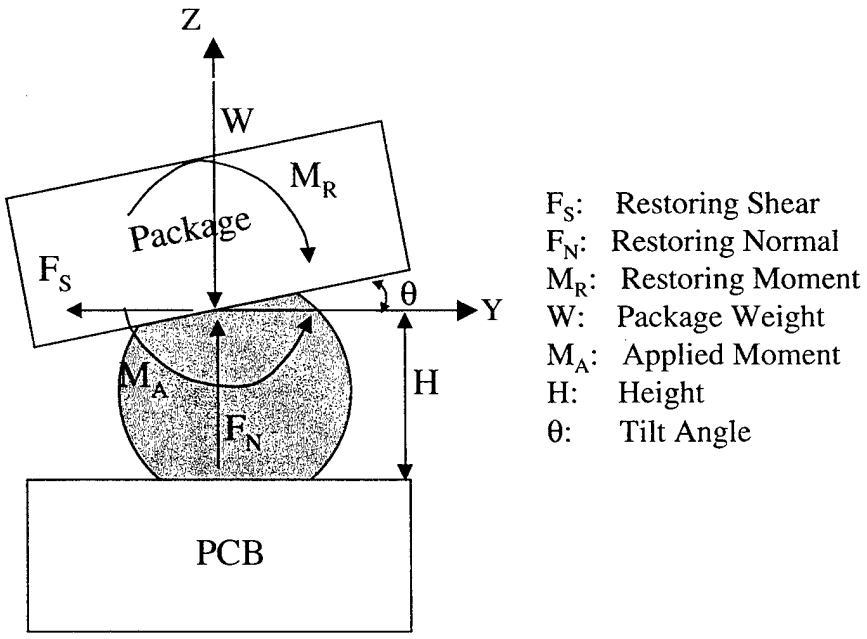

Figure 3.4 Energy balance for tilted solder joint.

3.3.2 Description of the Warpage

The warpage of the PCB or the package can be mathematically described as the implicitly defined surface:

$$f(X,Y,Z)=0 \tag{3.1}$$

where, the warpage magnitude Z varies from one solder joint location to another. Now, we can assign a local coordinate system to the bottom/top pad of each solder joint. Assuming initially that there is no warpage, and therefore the local axes are aligned with the global coordinate axes, the transformation due to the PCB warpage can be described as a rotation matrix:

$$R_w = \begin{bmatrix} n_X^x & n_X^y & n_X^z & 0 \\ n_Y^x & n_Y^y & n_Y^z & 0 \\ n_Z^x & n_Z^y & n_Z^z & 0 \\ 0 & 0 & 0 & 1 \end{bmatrix} \tag{3.2}$$

Where, the non-zero terms in the first three columns are the direction cosines of the transformed local coordinate axes with respect to the global axes denoted by the subscripts. Since the gradient of the warped surfaced defined by Equation 3.1 points in a direction normal to the surface, the following is true:

$$\mathbf{n}^{\mathbf{z}} = \begin{Bmatrix} n_X^z \\ n_Y^z \\ n_Z^z \end{Bmatrix} = \frac{\nabla f}{|\nabla f|} \tag{3.3}$$

Now, the only requirement for the two vectors $\mathbf{n}^{\mathbf{x}}$ and $\mathbf{n}^{\mathbf{y}}$ (defined similar to $\mathbf{n}^{\mathbf{z}}$ above) is that they lie in the tangent plane defined by the set of points $\boldsymbol{s}$ such that:

$$\nabla f \cdot \mathbf{s} = \mathbf{0} \tag{3.4}$$

Assuming without any loss of generality that the intersection of the above tangent plane with a plane parallel to the global X-Z plane as the direction of the new local x-axis, we can define $\mathbf{n}^{\mathbf{x}}$ as:

$$\mathbf{n}^{\mathbf{x}} = \begin{Bmatrix} n_X^x \\ n_Y^x \\ n_Z^x \end{Bmatrix} = \begin{Bmatrix} \dfrac{n_Z^z}{\sqrt{(n_Z^z)^2 + (n_X^z)^2}} \\ 0 \\ -\dfrac{n_X^z}{\sqrt{(n_Z^z)^2 + (n_X^z)^2}} \end{Bmatrix} \qquad 3.5$$

Clearly, with the above definition, $\mathbf{n}^{\mathbf{x}}$ is orthogonal to $\mathbf{n}^{\mathbf{z}}$. Finally, $\mathbf{n}^{\mathbf{y}}$ can be obtained as the cross product:

$$\mathbf{n}^{\mathbf{y}} = \mathbf{n}^{\mathbf{z}} \times \mathbf{n}^{\mathbf{x}} \qquad 3.6$$

If the function had been defined parametrically, as is customary in the field of geometric modeling (Mortensen, 1997), then the surface definition of Equation 3.1 would be in terms of two parameters u and v in the range [0,1]:

$$\mathbf{S}(u,v) = \begin{Bmatrix} X(u,v) \\ Y(u,v) \\ Z(u,v) \end{Bmatrix} \qquad 3.7$$

The vectors $\mathbf{n}^{\mathbf{x}}$, $\mathbf{n}^{\mathbf{y}}$ and $\mathbf{n}^{\mathbf{z}}$ are easily obtained from this parametric definition as:

$$\mathbf{n}^{\mathbf{x}} = \frac{\partial \mathbf{S}}{\partial u}, \quad \mathbf{n}^{y} = \frac{\partial \mathbf{S}}{\partial v} \quad \text{and} \quad \mathbf{n}^{\mathbf{z}} = \mathbf{n}^{\mathbf{x}} \times \mathbf{n}^{\mathbf{y}} \qquad 3.8$$

3.3.3 Description of the Package Configuration

The package can in general translate and rotate relative to its original configuration during the self-assembly process. The rotation of the package can be defined about an arbitrary spatial axis originating at the centroid and described by its

three direction cosines. This rotation can be easily visualized as a sequence of rotations about the three coordinate axes. The result of the procedure is a composite rotation matrix:

$$R_p = R_X(\gamma) * R_Y(\beta) * R_Z(\alpha) \qquad 3.9$$

Where the R's are the standard rotation matrices in homogeneous coordinates (Craig, 1989):

$$R_Z(\alpha) = \begin{bmatrix} Cos(\alpha) & -Sin(\alpha) & 0 & 0 \\ Sin(\alpha) & Cos(\alpha) & 0 & 0 \\ 0 & 0 & 1 & 0 \\ 0 & 0 & 0 & 1 \end{bmatrix}$$

$$R_Y(\beta) = \begin{bmatrix} Cos(\beta) & 0 & Sin(\beta) & 0 \\ 0 & 1 & 0 & 0 \\ -Sin(\beta) & 0 & Cos(\beta) & 0 \\ 0 & 0 & 0 & 1 \end{bmatrix}$$

$$R_X(\gamma) = \begin{bmatrix} 1 & 0 & 0 & 0 \\ 0 & Cos(\gamma) & -Sin(\gamma) & 0 \\ 0 & Sin(\gamma) & Cos(\gamma) & 0 \\ 0 & 0 & 0 & 1 \end{bmatrix}$$

$R_Z(\alpha)$ is the transformation matrix that rotates the axis α-deg about the reference z-axis and places the rotation axis in x-z plane of the reference coordinate system. $R_Y(\beta)$ is the transformation matrix that rotates the axis β-deg about the reference y-axis and makes it coincident with reference x-axis. $R_X(\gamma)$ is the transformation matrix that rotates the package γ-deg CCW about the reference x-axis. The three angles α,β,γ are the unknowns to be determined to describe the equilibrium orientation of the package.

The translation of the package, which in turn will be imposed on the top pads of the solder joints, can be expressed as:

$$T_p = \begin{bmatrix} 1 & 0 & 0 & T_X \\ 0 & 1 & 0 & T_Y \\ 0 & 0 & 1 & T_Z \\ 0 & 0 & 0 & 1 \end{bmatrix}$$

Where, the last column contains the translations of the package centroid in the three coordinate directions. These translations are again unknowns that need to be determined. Combining the translation and rotation of the package, the composite transformation of the package is obtained as:

$$T_c = T_p R_p \qquad 3.10$$

Where, the order of the operations ensures that rotation is carried out prior to translation.

3.3.4 Restoring Forces and Moments

Surface energy minimization theory for predicting molten solder droplet shape is well established at the present time (see Heinrich (1997) for a survey, and Subbarayan (1996) for a specific example). In the present study, the *Surface Evolver* code was used to predict the shapes (Brakke, 1994). Given a user-defined initial surface, the program evolves toward a minimum energy profile by using a gradient descent method on a space of admissible surfaces to try to find the local minimum of the energy function. The energies of relevance for a droplet are surface tension and gravitational energies. For solder joint applications the gravitational energy of the droplet itself is small compared to the surface energy and can be ignored. Thus, under quasi-static conditions, the restoring normal and shear forces generated by the solder

joint can be calculated as the derivatives of energy with respect to a motion in the required directions:

$$F_S = \frac{\partial E}{\partial P}_{H=Const} \approx \sigma \frac{\partial A}{\partial P}_{H=Const} \quad 3.11$$

$$F_N = \frac{\partial E}{\partial H}_{P=Const} \approx \sigma \frac{\partial A}{\partial H}_{P=Const} \quad 3.12$$

$$E = \int_A \sigma dA \quad 3.13$$

where F_S, F_N are the shear and normal restoring forces respectively (see Fig. 3.4). P is the misalignment, H is the solder joint height, E is the local minimum energy of the solder joint, A is the local minimum area, and σ is the surface tension coefficient which is assumed to be constant at every point on the surface. In addition to the restoring forces, a restoring moment, M_R, also exists:

$$M_R = \frac{\partial E}{\partial \theta} \approx \sigma \frac{\partial A}{\partial \theta} \quad 3.14$$

For a given set of solder parameters: pad dimensions, solder volume, solder height, and pad rotation, *Surface Evolver* determined the stable shape after iterative computations and calculated the restoring forces and moments. The surface tension coefficient value was 350 dyne/cm, a value most commonly used for eutectic Sn/Pb solder and most other solder materials (Tower, et al., 1999).

Since the package may contain numerous solder joints each with its own set of parameter values, regression models were developed to calculate the restoring forces and moments. The models were developed using a commercially available

multiple regression-based analysis tool *DOE KISS* (Design-Of-Experiment Keep-It-Simple-Statistically) for Microsoft Excel (Digital Computations, 1997). A 3-level/3 factor (3^3) full factorial designed experiment was used to generate the force and moment models. The misalignment was ignored in building the regression model to reduce the computational expense. While this would lead to an inaccurate solution, it was felt that this inaccuracy would be small for small amounts of warpage or volume variations. The factors and their levels are shown in Table 3.1

Table 3.1 DOE factors.

Factor	Level 1	Level 2	Level 3
A. Solder Volume $(mm)^3$	5.15 E-2	5.90 E-2	6.65 E-2
B. Solder Height (mm)	0.275	0.400	0.525
C. Solder Pad Tilt, θ (deg)	-5	0	+5

The results of the 27 runs are shown in Table 3.2. The force and moment data were generated during each *Evolver* run. The force and moment models generated by *DOE KISS* give explicit relations (polynomial form) between the force and moment values and the design parameters of the solder joint. These models are listed below:

$$F_S = -0.55590*C - 0.16027*A*C + 0.98538*A*C + 0.00895A*B*C + 0.03992*A^2*C - 0.48075*B^2*C \quad 3.15$$

$$F_N = -15.896 + 7.33854*A - 34.401*B - 4.78442*A*B - 0.58688*A^2 + 21.347*B^2 - 1.01196*C^2 + 1.56582*A^2*B - 1.18379*A*B^2 - 0.97894*A*C^2 + 1.58117*B*C^2 \quad 3.16$$

$$M_R = -0.02326*C + 0.02584*A*C - 0.04513*B*C - 0.04717A*B*C + 0.01046*A^2*C + 0.06021*B^2*C \quad 3.17$$

The volume, height, and rotation values in the equations above are the non-dimensional or coded value of the parameters. The R^2 value characterizing the goodness of the fit is 0.9993 for the shear restoring force. It is 0.9994 for the normal restoring force and 0.9069 for the restoring moment.

Table 3.2 DOE results.

	Factors			Results		
Experiment	Volume (cm^3)	Height (cm)	Tilt (deg)	Shear Force (dyne)	Normal Force (dyne)	X-Moment (dyne-cm)
1	0.0000665	0.0525	5	-0.132642	-27.0194	-0.006742
2	0.0000665	0.0525	0	0.000000	-27.0667	0.000000
3	0.0000665	0.0525	-5	0.132640	-27.0194	0.006742
4	0.0000665	0.04	5	-0.776000	-10.1411	-0.021588
5	0.0000665	0.04	0	0.000000	-10.1645	0.000000
6	0.0000665	0.04	-5	0.776000	-10.1411	0.021588
7	0.0000665	0.0275	5	-2.081600	43.9081	0.187852
8	0.0000665	0.0275	0	0.000000	50.47	0.000000
9	0.0000665	0.0275	-5	2.081600	43.9081	-0.187852
10	0.000059	0.0525	5	-0.021000	-28.2353	-0.001176
11	0.000059	0.0525	0	0.000000	-28.2737	0.000000
12	0.000059	0.0525	-5	0.021000	-28.2353	0.001176
13	0.000059	0.04	5	-0.537000	-17.1968	-0.017277
14	0.000059	0.04	0	0.000000	-17.2557	0.000000
15	0.000059	0.04	-5	0.537000	-17.1936	0.017277
16	0.000059	0.0275	5	-2.071200	37.746	0.069080
17	0.000059	0.0275	0	0.000000	39.8438	0.000000
18	0.000059	0.0275	-5	2.071200	37.746	-0.069080
19	0.0000515	0.0525	5	0.079690	-28.4622	0.004286
20	0.0000515	0.0525	0	0.000000	-28.487292	0.000000
21	0.0000515	0.0525	-5	-0.079690	-28.4622	-0.004286
22	0.0000515	0.04	5	-0.274866	-23.4961	-0.010000
23	0.0000515	0.04	0	0.000000	-23.57	0.000000
24	0.0000515	0.04	-5	0.274866	-23.4961	0.010000
25	0.0000515	0.0275	5	-1.833460	25.28346	0.010200
26	0.0000515	0.0275	0	0.000000	26	0.000000
27	0.0000515	0.0275	-5	1.833460	25.28346	-0.010200

3.3.5 Transformation to Reference Solder Joint Configuration

The steps involved in transforming the solder droplet to the reference configuration, taking into account the package rotation and the PCB warpage are as follows:

1. Transform the top pad orientation to account for package warpage and package motion:

$$R_1 = T_c R_{wp} \tag{3.18}$$

where R_{wp} is the rotation due to warpage described in Equation 3.2 and T_c is as described in Equation 3.10.

2. Apply the following rotation to the top and bottom pads so that the bottom pad is aligned with the global axes and only the top pad is rotated.

$$R_2 = R_{wb}^{-1} R_1 \qquad 3.19$$

where R_{wb} is rotation due to the warpage of the PCB.

3. Rotate the droplet about the global z-axis until an orientation is reached in which the rotation of the top pad may be expressed as a rotation about the global x-axis. That is, the same final orientation R_3 of the top-pad is to be achieved by the following two equivalent rotations:

$$R_3 = R_Z(\theta_z) R_2 = R_X(\theta_x) \qquad 3.20$$

where

$$R_Z(\theta_z) = \begin{bmatrix} Cos(\theta_z) & -Sin(\theta_z) & 0 & 0 \\ Sin(\theta_z) & Cos(\theta_z) & 0 & 0 \\ 0 & 0 & 1 & 0 \\ 0 & 0 & 0 & 1 \end{bmatrix}$$

$$R_X(\theta_x) = \begin{bmatrix} 1 & 0 & 0 & 0 \\ 0 & Cos(\theta_x) & -Sin(\theta_x) & 0 \\ 0 & Sin(\theta_x) & Cos(\theta_x) & 0 \\ 0 & 0 & 0 & 1 \end{bmatrix}$$

Equating the direction cosine with respect to the z-axis of each transformation matrix, that is, the coefficients of the third columns of $R_X(\theta_x)$ and $R_Z(\theta_z)R_2$, we get three consistent equations in the two unknowns θ_X and θ_Z:

$$r_{13}\,\mathrm{Cos}(\theta_z) - r_{23}\,\mathrm{Sin}(\theta_z) = 0 \qquad 3.21$$

$$r_{13}\,\mathrm{Sin}(\theta_z) + r_{23}\,\mathrm{Cos}(\theta_z) = -\mathrm{Sin}(\theta_x) \qquad 3.22$$

$$r_{33} = \mathrm{Cos}(\theta_x) \qquad 3.23$$

Where, r_{ij} are the ijth terms of the R_2 matrix. The orthonormality of the R_2 matrix ensures the consistency of the above three equations. Thus, the rotation about the x-axis to be input into the regression model is simply,

$$\theta_x = \text{Cos}^{-1}(r_{33}) \qquad 3.24$$

3.3.6 Warpage Types

There are many choices for the nature of warpage in PCBs that can be used for the demonstration of the developed methodology. In the present study, experimental observations from literature were used to guide warpage pattern selection. Amagai observed warpage of a Micro-Star™ (μ*) BGA CSP post-assembly at 25 °C (Amagai, 1999). He then correlated the magnitude of assembly warpage to solder joint life through Finite Element Analysis (FEA). The correlation was strong. Of significance to the present study, the warpage of the PCB post-assembly was arch-type and was in the 9 to 15 μm range.

However, in the present study, the focus is restricted to the co-planarity of the package/component and PCB during the reflow process. The reflow temperature of eutectic solder is around 220°C. Figure 3.5 shows a relatively flat package at this temperature, hence, no warpage is present. Experiments conducted on PCBs by Sutherline, et al. (1998), showed a bowl-type maximum out-of-plane displacement difference of 0.629 mm for a 203.2 mm x 177.8 mm x 1.524 mm thick PCB with traces at 220°C using infrared reflow. The combined non-zero flatness of the package and PCB are shown in Figure 3.6 for which we assumed a 25 μm bowl-shaped warpage of the PCB. Non-symmetric warpage was modeled by allowing the

right or left side warpage, as measured from the package centerline, to vary from 0 to 25 μm (see Fig. 3.6).

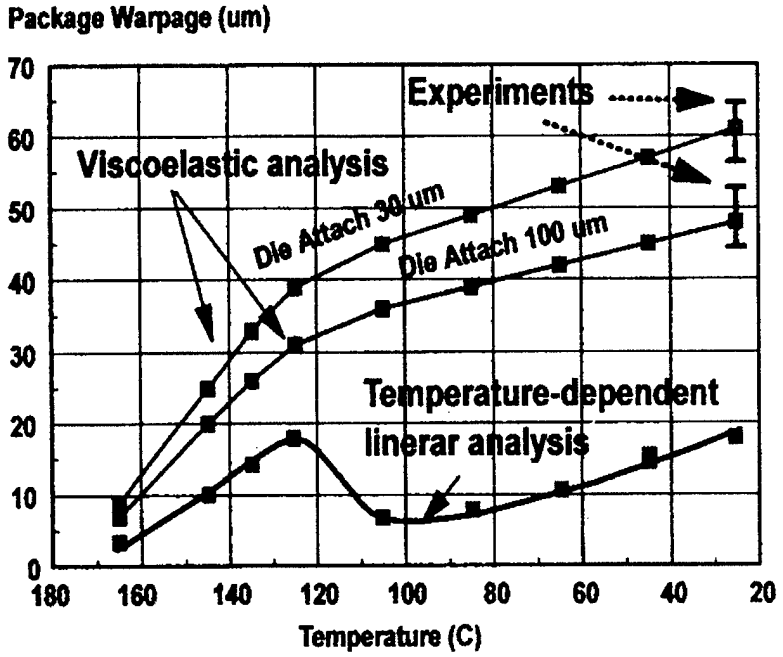

Figure 3.5 Package warpage for "μ*BGA" CSP (Amagai, 1999)

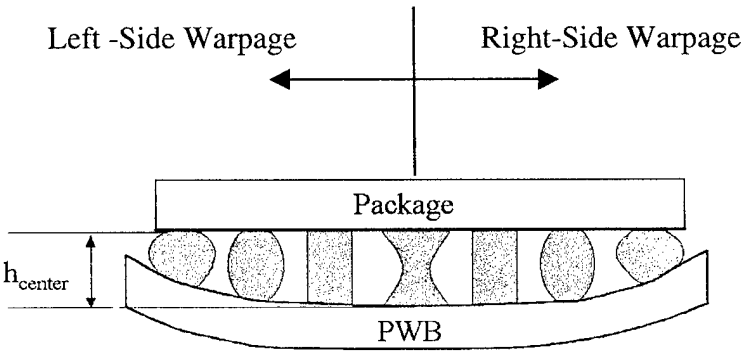

Figure 3.6 Combined warpage of package and PWB during reflow.

3.3.7 The Optimization Algorithm

The developed methodology requires six optimization parameters to describe package rotation about its rotation axis (3 parameters) and package translation (3 parameters). Here, since the regression model was simplified by ignoring misalignment, fewer parameters were required. Thus, the package equilibrium optimization problem may be formally posed as:

Find the equilibrium height, h, tilt axis, and degree of tilt of the package $f(h,\alpha,\beta,\gamma)$ so that:

$$\mathbf{F}_{\text{package}} - \sum_i (\mathbf{F}_{\text{Ni}} + \mathbf{F}_{\text{Si}}) = \mathbf{0} \qquad 3.25$$

$$\sum_i \left[\mathbf{M}_{\text{Ri}} + \Delta\mathbf{X}_{\text{i}} \times (\mathbf{F}_{\text{Ni}} + \mathbf{F}_{\text{Si}})\right] = \mathbf{0} \qquad 3.26$$

where $\mathbf{F}_{package}$ is the externally applied force on the package (including its weight), and $\mathbf{F}_{Ni}$ and $\mathbf{F}_{Si}$ are the normal and shear restoring force vectors at joint i. $\Delta\mathbf{X}_i$ is the distance from the solder joint to the point about which the moment is calculated. The above two vector equations are equivalent to a total of six scalar equations. The nonlinear equation solution was reformulated in the present study as an optimization problem so an approximate solution that may not satisfy the equations exactly is also allowed. The objective in the optimization is to minimize the least squared error in the above equations. The solution was determined, starting from a level package configuration using the NLPQL code (Schittkowski, 1985). This code iteratively improved the design until the optimum point was reached. The NLPQL routine finds the minimum or maximum of a nonlinear function of n optimization parameters subject to nonlinear or linear constraints using a Sequential Quadratic

Programming (SQP) method. The gradients were calculated at each iteration by forward differences. For an assembly with a given warpage level, the algorithm to calculate the heights of all the solder joints and package tilt is shown in the flowchart. The height of the solder joints due to warpage is calculated using

$$Z(X,Y) = Z_{center} - \Delta Z\,(X^2 + Y^2)/L_{pckg} \qquad 3.27$$

The warpage is characterized by the vertical height variation (ΔZ) across the diagonal length (L_{pckg}) of the package. Figure 3.7 illustrates the flow of control within the developed procedure.

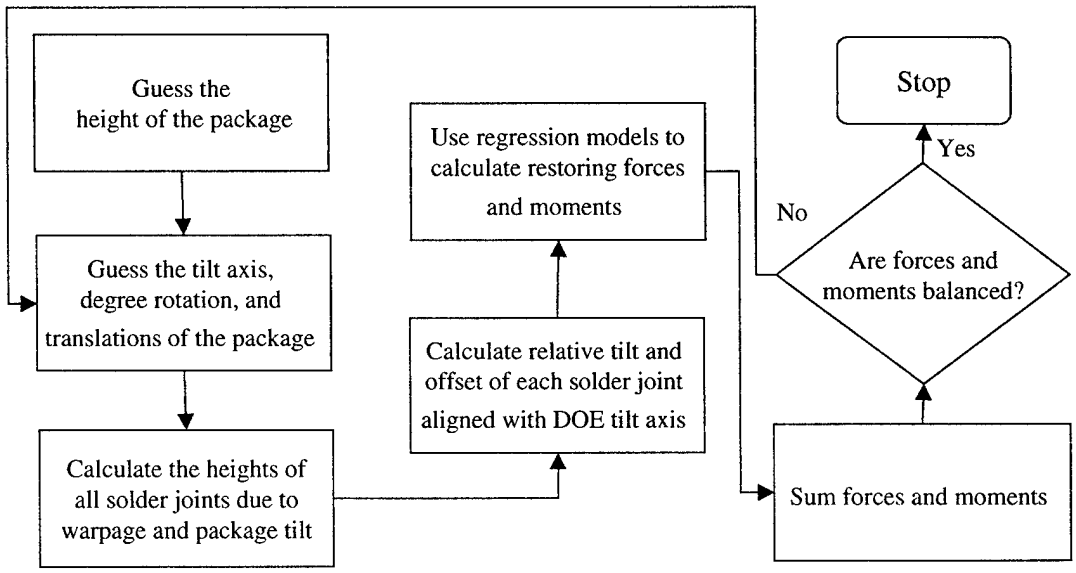

Figure 3.7 Flow of control in program.

3.3.8 Validation of the Model

The hypothetical 3x3 area-array electronic package was used to test the code. Eight test cases were selected based on variations in volume and warpage:

1. Constant volume - no warpage
2. Constant volume – 25 μm left warpage/0 μm right warpage

3. Constant volume – 0 μm left warpage/25 μm right warpage
4. Constant volume – 25 μm left warpage/25 μm right warpage
5. Volume varies linearly from left to right – no warpage →
6. Volume varies linearly from top to bottom – no warpage ↓
7. Volume varies linearly from left top corner to right bottom corner – no warpage ↘
8. Volume varies linearly from left bottom corner to right top corner – no warpage ↗

The results of the test cases are shown in Table 3.3 and Figures 3.8-3.15. The equilibrium configuration for each test was exactly as predicted.

Table 3.3 Test results (V = Mean Volume (5.90E-5 cm^3)).

	Volume (cm^3)			Final Height (cm)			Final Tilt (deg)		
Test #1	1.00*V	1.00*V	1.00*V	0.035	0.035	0.035	0	0	0
	1.00*V	1.00*V	1.00*V	0.035	0.035	0.035	0	0	0
	1.00*V	1.00*V	1.00*V	0.035	0.035	0.035	0	0	0
Test #2	1.00*V	1.00*V	1.00*V	0.0343	0.0356	0.0347	0.3314	0.1252	0.1200
	1.00*V	1.00*V	1.00*V	0.0355	0.0357	0.0347	0.1666	0.1200	0.1200
	1.00*V	1.00*V	1.00*V	0.0343	0.0356	0.0347	0.3314	0.1252	0.1200
Test #3	1.00*V	1.00*V	1.00*V	0.0347	0.0356	0.0343	0.1200	0.1252	0.3314
	1.00*V	1.00*V	1.00*V	0.0347	0.0357	0.0355	0.1200	0.1200	0.1666
	1.00*V	1.00*V	1.00*V	0.0347	0.0356	0.0343	0.1200	0.1252	0.3314
Test #4	1.00*V	1.00*V	1.00*V	0.0342	0.0354	0.0342	0.4051	0.2865	0.4051
	1.00*V	1.00*V	1.00*V	0.0354	0.0367	0.0354	0.2865	0.0004	0.2865
	1.00*V	1.00*V	1.00*V	0.0342	0.0354	0.0342	0.4051	0.2865	0.4051
Test #5	1.04*V	1.00*V	0.96*V	0.0356	0.0350	0.0343	0.0795	0.0795	0.0795
	1.04*V	1.00*V	0.96*V	0.0356	0.0350	0.0343	0.0795	0.0795	0.0795
	1.04*V	1.00*V	0.96*V	0.0356	0.0350	0.0343	0.0795	0.0795	0.0795
Test #6	1.04*V	1.04*V	1.04*V	0.0356	0.0356	0.0356	0.0795	0.0795	0.0795
	1.00*V	1.00*V	1.00*V	0.0350	0.0350	0.0350	0.0795	0.0795	0.0795
	0.96*V	0.96*V	0.96*V	0.0343	0.0343	0.0343	0.0795	0.0795	0.0795
Test #7	1.04*V	1.02*V	1.00*V	0.0357	0.0353	0.0350	0.0562	0.0562	0.0562
	1.02*V	1.00*V	0.98*V	0.0353	0.0350	0.0346	0.0562	0.0562	0.0562
	1.00*V	0.98*V	0.96*V	0.0350	0.0346	0.0343	0.0562	0.0562	0.0562
Test #8	1.00*V	0.98*V	0.96*V	0.0350	0.0346	0.0343	0.0562	0.0562	0.0562
	1.02*V	1.00*V	0.98*V	0.0353	0.0350	0.0346	0.0562	0.0562	0.0562
	1.04*V	1.02*V	1.00*V	0.0357	0.0353	0.0350	0.0562	0.0562	0.0562

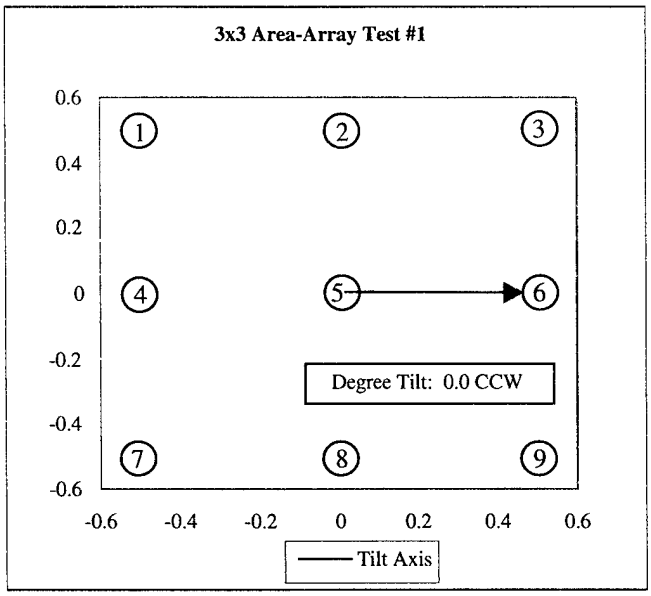

Figure 3.8 Test #1 results showing tilt axis and degree tilt.

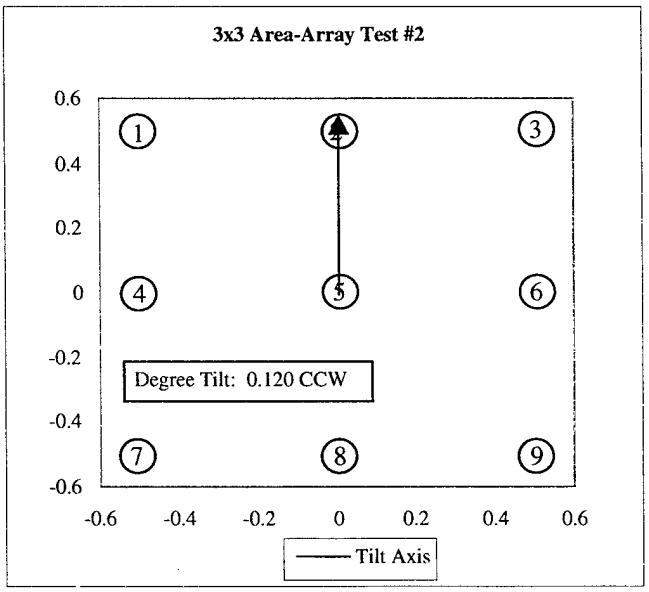

Figure 3.9 Test #2 results showing tilt axis and degree tilt.

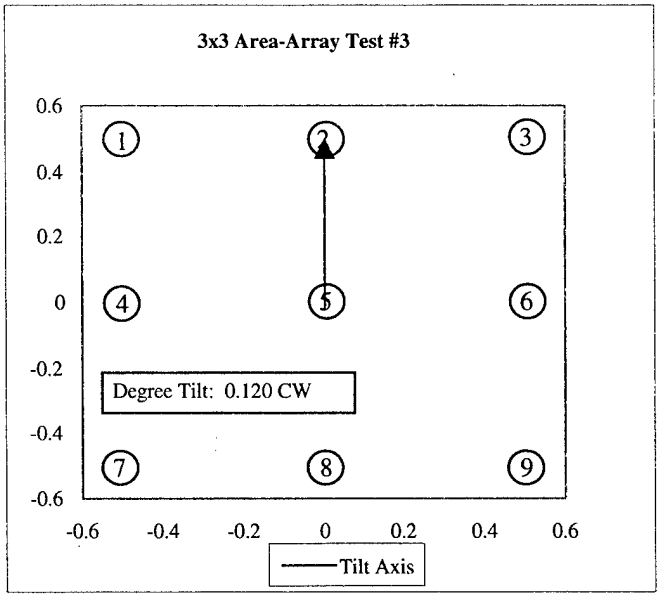

Figure 3.10 Test #3 results showing tilt axis and degree tilt.

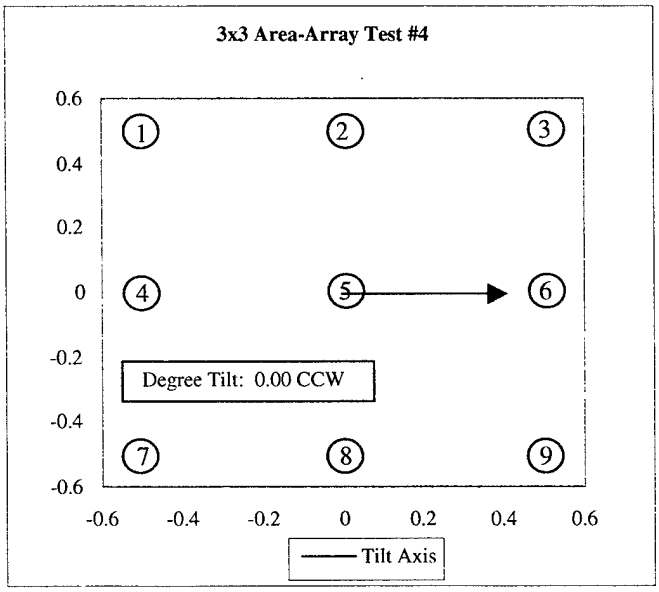

Figure 3.11 Test #4 results showing tilt axis and degree tilt.

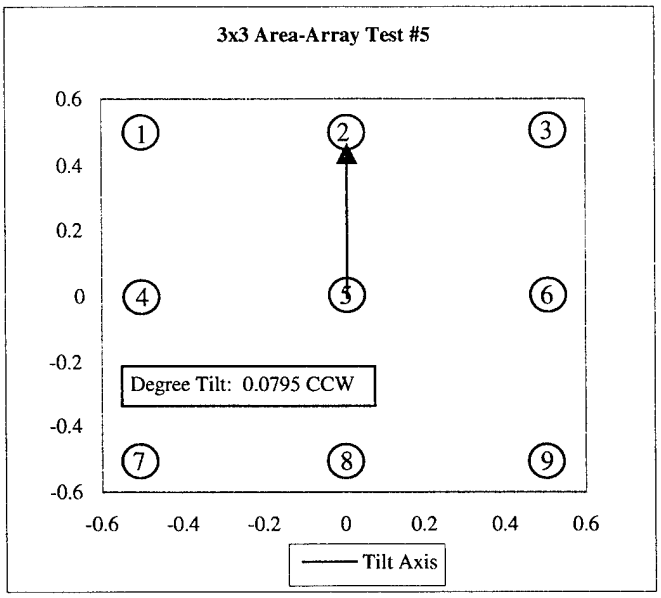

Figure 3.12 Test #5 results showing tilt axis and degree tilt.

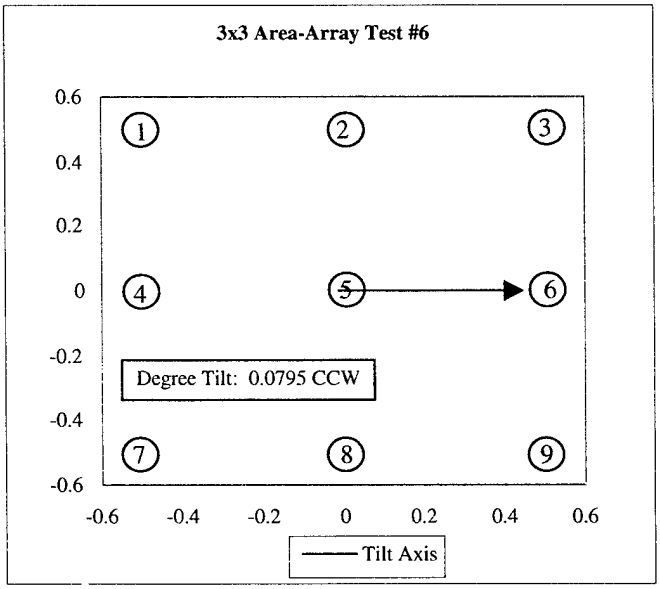

Figure 3.13 Test #6 results showing tilt axis and degree tilt.

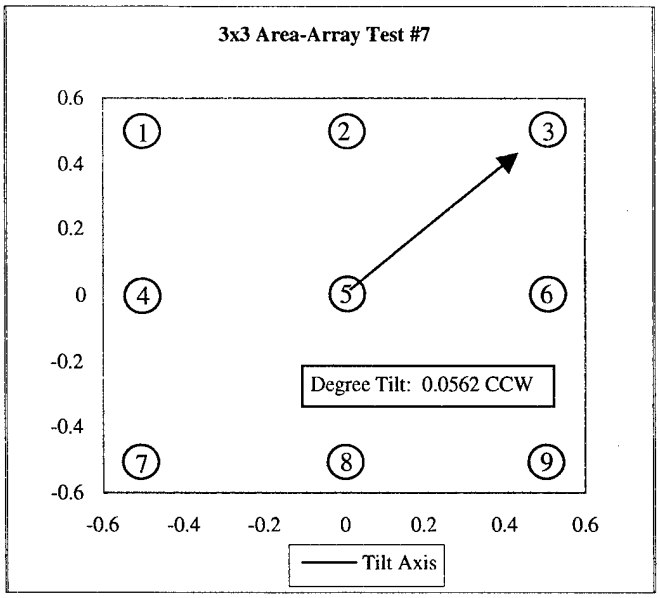

Figure 3.14 Test #7 results showing tilt axis and degree tilt.

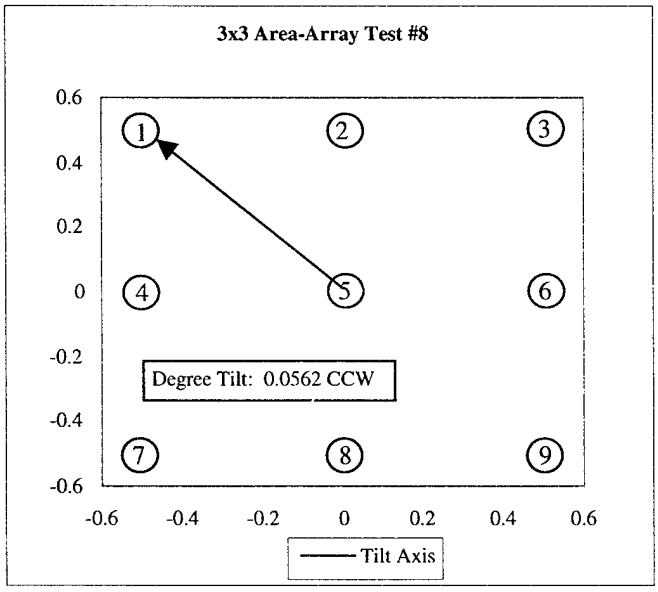

Figure 3.15 Test #8 results showing tilt axis and degree tilt.

3.4 Conclusions

The research has demonstrated a methodology for predicting the final equilibrium configuration for area-array packages with warped solder joints during solder reflow. This technique is novel in its application of homogeneous transformation theory to electronic packages and the use package rotation as an optimization parameter to determine package equilibrium in the presence of symmetric and non-symmetric warpage.

The methodology has been modified to include package warpage and solder joint misalignment. The application of the methodology to determine the thermal stress/strain distribution in the most susceptible joint, and the fatigue life of the most susceptible or any other selected solder joints in a "hypothetical" electronic package will be demonstrated in Chapter 4.

Chapter 4

A Methodology For Assessing The Reliability Of Warped Solder Joints In Area-Array Packages

4.1 Chapter Overview

In this chapter we introduce a novel methodology for studying the effect of warpage on solder joint reliability. The methodology consists of combining the solder shape prediction methodology introduced in Chapter 3 with the decomposed analysis technique discussed in Chapter 2 to determine the equilibrium configuration of an area-array package with warped solder joints and assessing the reliability of these warped joints.

Finally, to illustrate the usefulness, flexibility and strength of this procedure, the procedure is demonstrated on a hypothetical three-dimensional electronic package with four solder joints.

The objectives of this chapter:

- Predict shape of solder joints in hypothetical area-array package using the shape prediction program discussed in Chapter 3.
- Apply decomposition technique to analyze a hypothetical area-array package with warped solder joints.

- Finally, to assess the reliability of warped solder joints.

4.2 Introduction

Reliability is one of the major concerns for ball grid array (BGA) assemblies. One common failure mechanism in these packages is low-cycle fatigue of solder joints. The fatigue life of solder joints depends on the stress/strain in the solder joints under the user environment. The stresses in turn depend on the shape of the solder joints. In package design and optimization, fatigue analysis derived by experiment, such as accelerated temperature cycling, is expensive and time consuming. A numerical model can reduce the product development cycles.

Restating from Chapter 3, the numerical model should consist of three critical steps:

1. solder joint shapes,
2. thermal stress/strain distribution in the most susceptible joint after solidification and during thermal cycling, and
3. fatigue lives of the most susceptible or any other selected solder joints.

The solder shape prediction model and the code demonstrated in Chapter 3 accomplish the first step. The thermal stress/strain calculation identifies the most susceptible solder joint and estimates its damage level after each temperature cycle. The accumulated damage level can be used to predict the fatigue life by using empirical models correlated to the large body of existing experimental data.

There have been many papers reporting calculation techniques for the above three steps. The research in this chapter demonstrates novel approaches for shape, stress/strain, and fatigue calculations. Since we have already discussed the

methodology for solder shape prediction in Chapter 3, this chapter will only consider stress/strain and fatigue calculations.

4.3 Methodology

4.3.1 Thermal Stress/Strain Models

Thermal stress/strain models have been well developed for surface mount technologies. It is common to use 2-D finite element modeling to simulate the structures of surface mount technologies (Barker, et al., 1993). For more complex BGA assemblies, 3-D finite element modeling is necessary to simulate every solder joint in order to identify the joint most susceptible to failure. However, full-scale 3-D modeling in not cost effective and is usually replaced by alternative modeling techniques like: 1) analytical model (Borgessen, et al., 1992), 2) 3-D sliced FE model (Nagarand and Mahakingam, 1993), 3) macro (global)/micro (local) FE model (Corbin, 1994, Cheng, et al, 1998, and Saito, et al., 1999), 4) Nested FE model (Darbha and Dasgupta, 1999), and 5) Decomposition model (Deshpande and Subbarayan, 2000). Zhang, et al., (1999) present an evaluation of the accuracy of 2-D and 3-D structural approximations (relative to experimental measurement) in the analysis of area-array packages.

In general, most existing analytical models cannot handle complicated, time-dependent deformation mechanisms such as creep. The 3-D sliced model cannot simulate all the solder joints. One common implementation of the macro (global)/micro (local) strategy replaces solder joints by equivalent, nonlinearly behaving beams in which the beam properties are calculated using a designed experiment based on the analysis of a three-dimensional solder model. Once the

equivalent beam has been formulated, a full-scale 3-D FE analysis of the entire assembly is performed identifying the most susceptible solder joint. A micro/local model then simulates the structure of that solder joint using a much finer mesh than the macro (global) model. The disadvantage to this approach is that any component or PCB change would require a complete re-analysis of the 3-D model with the equivalent beams. The nested FE model (NFEM) uses colonies of nested sub-elements that are created inside a main element to capture localized large gradients of stress and strain. Once again, any change to the assembly would require re-analysis of a full 3-D FE mesh. The decomposition model, discussed in Chapter 2, is free from the macro (global)/micro (local) and NFEM disadvantages since the component and PCB are separate subsystems and any changes would simply require the rebuilding of that subsystem model alone. However, none of the models above appear to have been used to analyze a package with warped solder joints. The decomposition technique, with its natural ability to accommodate variations in subsystems may allow one to study the effects of warped solder joints efficiently. In implementing a decomposed analysis strategy to study warpage effects on solder joint reliability, the only real need is for a new regression model for solder work that incorporates design, analysis and manufacturing parameters. This is since an assumption is made in the present study that the stiffness matrices of PCB and component are not altered by their warpage. That is, the geometrical changes caused by warpage are small enough that they don't alter structural behavior.

4.3.2 Numerical Simulations to Approximate Solder Joint Response

A statistically designed set of simulations is carried out next to capture the nonlinear response of the solder joints to changes in design, analysis, and manufacturing related variables. For this modeled response to be valid for the widest possible choice of future and present packages, careful thought must be given to the input parameters and their ranges.

In the present study, the analysis parameter included the solder relative shear displacement. A range of 1.0 to 3.0 microns is chosen for the relative shear displacement (u). Due to the size of the package and FE analysis results, the solder joint bending, normally represented by a rotation of the top pad, was neglected. In addition, work due to local mismatch at each interface and relative axial displacement is ignored and set equal to the solder free expansion since it is believed, and past simulations have shown, that the global relative shear and bending were dominant.

Solder height and volume parameters were chosen for the study. These parameters are normally considered design parameters along with solder pad diameter, however, manufacturing variations, which include warpage and solder volume variation, can affect the height of the solder joint. Therefore, the present research will classify these parameters as design/manufacturing parameters. Three different values (levels) of the variables were selected. These values were assumed to be uniformly distributed about the nominal value in a range of ±20 percent for volume and ±18 percent for height. This choice of the range was motivated by a belief that even within a reasonably small range around the nominal value, an

optimal solution other than the nominal solution must exist. For this study, the solder upper and lower pad diameters are held constant.

One *pure* manufacturing parameter, pad tilt of individual solder joints *during reflow* due to warpage, was chosen for the study. The warpage represented by the angle θ_{warp} was assumed to have a range of 0.0° to 3.0°. The parameters (factors) and levels are shown in Table 4.1.

Table 4.1 Factors and levels.

Factor	Level 1	Level 2	Level 3
A: Volume (V/V_0)	1.20	1.00	0.80
B: Height (H/H_0)	1.18	1.00	0.82
C: Pad Tilt due to Warpage (deg)	0.00	1.50	3.00
D: Relative Shear Displacement (μm)	1.00	2.00	3.00
$V_0 = 2.5$ E8 μm^3			
$H_0 = 550$ μm			

It is parenthetically noted that to build a global approximation in a problem with a large number of variables, a partial (fractional) factorial experiment such as an orthogonal array of Taguchi (Peace, 1993) may be more appropriate for economy of analysis. A designed experiment using a Taguchi L27 orthogonal array based on three levels of design, analysis, and manufacturing variables, as shown in Table 4.2, was used to capture the response of the solder joint.

Table 4.2 The fractional designed experiment used to build the regression model for solder work.

Factor	A	B	C	D	
Run	Volume	Height	Warpage (deg)	Shear (mm)	Work (N-mm)
1	0.80	0.82	0	1	1.8380
2	0.80	0.82	1.5	1	1.8429
3	0.80	0.82	3	1	1.8565
4	0.80	1.00	0	2	4.1110
5	0.80	1.00	1.5	2	4.1180
6	0.80	1.00	3	2	4.1280
7	0.80	1.18	0	3	5.9770
8	0.80	1.18	1.5	3	5.9670
9	0.80	1.18	3	3	5.9360
10	1.00	0.82	0	2	5.4920
11	1.00	0.82	1.5	2	5.4590
12	1.00	0.82	3	2	5.5050
13	1.00	1.00	0	3	8.1220
14	1.00	1.00	1.5	3	8.0030
15	1.00	1.00	3	3	8.2080
16	1.00	1.18	0	1	1.2311
17	1.00	1.18	1.5	1	1.2392
18	1.00	1.18	3	1	1.2236
19	1.20	0.82	0	3	10.3420
20	1.20	0.82	1.5	3	10.5040
21	1.20	0.82	3	3	10.3260
22	1.20	1.00	0	1	1.6764
23	1.20	1.00	1.5	1	1.6887
24	1.20	1.00	3	1	1.6738
25	1.20	1.18	0	2	3.9680
26	1.20	1.18	1.5	2	3.9860
27	1.20	1.18	3	2	3.9890

A non-linear elastic-plastic analysis was performed on each of the twenty-seven settings in the designed experiment using a new *Surface Evolver* script that produces a 3-D FE surface mesh of *Evolver's* solder profile for import into the IDEAS finite element code. The IDEAS code is used to generate the 3-D finite element solid mesh. The 3-D finite element mesh is analyzed using the ABAQUS finite element code. A typical finite element model of the solder joint generated by using this methodology is shown in Figure 4.1. The model incorporates over 1700 tetrahedral 3-D solid elements. The accelerated test condition consists of a two

minutes linear temperature loading ramp with no dwell period and the temperature range is from 0 °C to 100 °C..

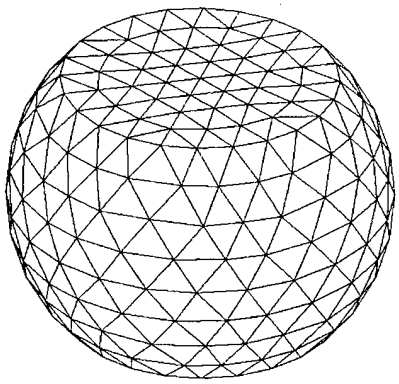

Figure 4.1 A typical FE model of the solder joint.

A linear regression model (Equation 4.1) was built using the commercial software *DOE KISS* to relate the work quantities with the four input parameters.

$$W = 4.75597 + 0.50607 * A - 0.83398 * B + 0.00491 * C + 3.11951 * D - 0.32930 * \mathrm{A} * \mathrm{B} + 0.51520 * \mathrm{A} * \mathrm{D} - 0.36337 * \mathrm{B} * \mathrm{D} \quad 4.1$$

The fit is accurate as measured by an R^2 value of 0.9984.

The relative displacement can be identified for each solder joint after temperature cycling. This can be used to calculate the stress/strain distributions and the associated inelastic dissipation terms with respect to temperature loading levels, rates, and frequencies. For this study, the calculation includes only elastic and rate-independent plastic behavior of solder. The output is used for fatigue life estimation.

4.3.3 Solder Joint Fatigue Life Calculation

Several fatigue indicators have been used to predict fatigue failure in solder joints. These include:

a. Maximum plastic strain (Corbin, 1993)

b. Plastic strain range (Nagaraj and Mahalingam, 1993)

c. Inelastic strain energy density (Darveaux, et al., 1995)

d. Strain energy partitioning, (Barker, et al., 1993).

Failure of ductile solder material arises from repeated nonlinear deformation. Previous studies have shown that strain energy density gives a very good correlation to solder crack growth data (Wong, et al, 1999). An empirically derived formula determined by Darveaux, et al. (1995) is modified and used in the current study to estimate fatigue life. The formula relates the amount of inelastic strain energy density developed during one temperature cycle (ΔW) to the number of cycles needed to induce solder failure, N_f, and is described below.

$$N_f \propto \frac{1}{\Delta W_{\text{int}}} \tag{4.2}$$

where ΔW_{int} is the inelastic strain energy density at the solder/package or solder/PWB interfaces.

To determine N_f from equation 4.2, we need to estimate ΔW_{int}. For Accelerated Temperature Cycling (ATC), the solder inelastic strain energy density at the end of the cycle and the inelastic strain energy density per cycle for each element, ΔW_{el}, can be obtained from the FE analysis of the solder model. Since failure usually occurs at the solder/package or solder/PWB interface, it is reasonable to assume the inelastic strain energy density is distributed equally between the two interfaces. The interfacial strain energy density per cycle is

$$\Delta W_{\text{int}} = \frac{\sum \Delta W_{el} V_{el}}{2V_{char}} \tag{4.3}$$

where:

ΔW_{el}: Inelastic Strain Energy Density/Element

V_{el}: Element Volume

V_{char}: Characteristic Volume at the solder/package or solder/PWB interface contributing to flaw growth

$V_{char} = Pad\ Area * Characteristic\ Length$

In this study, V_{char} is the same for each solder joint, therefore,

$$N_f \propto \frac{1}{\sum \Delta W_{el} V_{el}} * SF = \frac{1}{Total\ Plastic\ Energy\ Dissipation} * SF \qquad 4.4$$

where *SF* is a Scale Factor used specifically for this study to generate whole number quantities for failure cycles. For this study, *SF* was set equal to 100,000. Since we only considered elastic and rate-independent plastic solder behavior, the applied loading on the solder joints consisted of a modified ATC specified by Darveaux. et al. (1995): two minutes linear temperature loading/unloading ramps with no dwell period and the temperature range is from 0 °C to 100 °C.

It is reasonable to expect that any quantity such as the inelastic dissipation calculated as a result of finite element analysis is dependent on finite element mesh size. Therefore, a mesh density study was performed to determine the appropriate mesh density for the solder model. The element edge lengths were varied for a nominal solder joint under a constant relative shear over the above temperature cycle. The characteristics of the nominal solder joint are:

a. Height = 550 μm

b. Volume = 2.5 E8 μm^3

c. Upper/Lower Pad Diameter = 600 μm

d. Relative Shear Displacement = 2.0 μm

The total inelastic energy dissipations and errors were plotted and are shown in Figure 4.2.

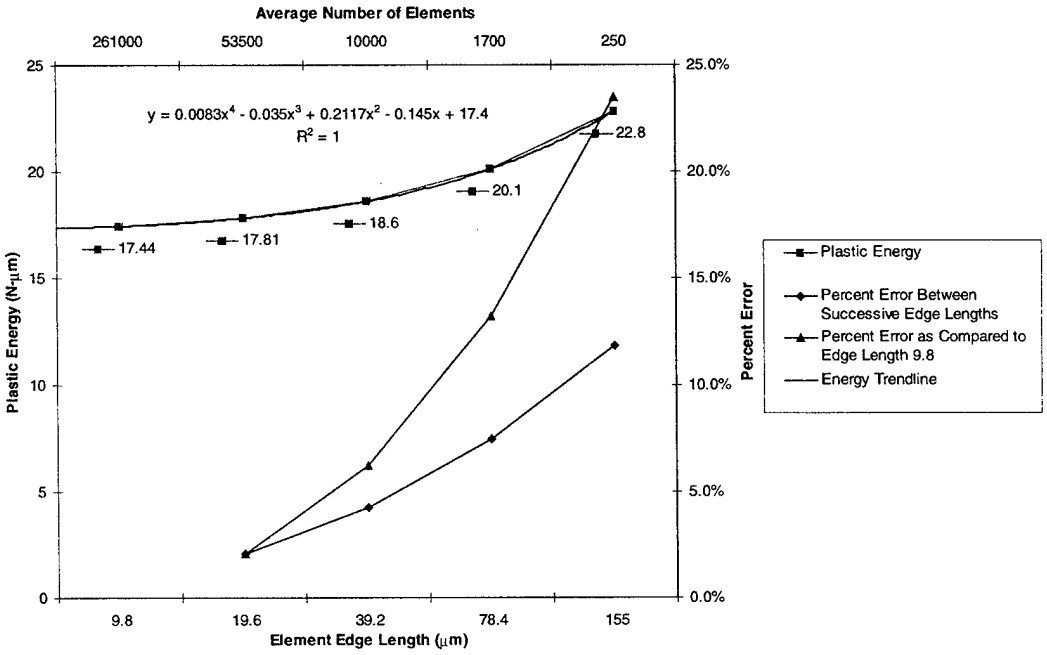

Figure 4.2 Mesh density study.

This study caused an element edge length of 36.2 μm (10,000 elements) being chosen for the solder joint models. The resulting plastic dissipation percent error as compared to element edge length of 9.8 μm (261,000 elements) is 6.24 percent, which is reasonable for this study.

A linear regression model (Equation 4.5) was built using *DOE KISS* to relate solder fatigue life with the four input parameters, volume, height, warpage tilt, and relative shear displacement,) for the 2x2 hypothetical warped model.

$$N_f = 5253.9 - 216.295 * A + 566.348 * B - 24.538 * C - 2796.2 * D + 2.782 * A * B * C - 802.0 * A * B * D - 15.121 * A * C * D^2 - 12.87 * \mathrm{B} * \mathrm{C} * \mathrm{D} \quad 4.5$$

The accuracy of the fit as measured by its R^2 value was 0.9813. The fatigue life expression is obtained from the original Taguchi L27 designed experiment based on three levels of design, analysis, and manufacturing variables listed in Table 4.1 and the solder joint FE model described in Figure 4.1. Results of the experiment is shown in Table 4.4

Table 4.3 The fractional designed experiment used to build the regression model for solder fatigue life.

Factor	A	B	C	D	
Run	Volume	Height	Warpage (deg)	Shear (mm)	Cycles to Failure
1	0.80	0.82	0	1	8658
2	0.80	0.82	1.5	1	8681
3	0.80	0.82	3	1	8518
4	0.80	1.00	0	2	5308
5	0.80	1.00	1.5	2	5342
6	0.80	1.00	3	2	5325
7	0.80	1.18	0	3	3971
8	0.80	1.18	1.5	3	3965
9	0.80	1.18	3	3	3935
10	1.00	0.82	0	2	4268
11	1.00	0.82	1.5	2	4202
12	1.00	0.82	3	2	4207
13	1.00	1.00	0	3	3056
14	1.00	1.00	1.5	3	3094
15	1.00	1.00	3	3	3045
16	1.00	1.18	0	1	8718
17	1.00	1.18	1.5	1	8688
18	1.00	1.18	3	1	8688
19	1.20	0.82	0	3	2509
20	1.20	0.82	1.5	3	2396
21	1.20	0.82	3	3	2430
22	1.20	1.00	0	1	8203
23	1.20	1.00	1.5	1	8065
24	1.20	1.00	3	1	8110
25	1.20	1.18	0	2	5230
26	1.20	1.18	1.5	2	5238
27	1.20	1.18	3	2	5222

In general, the ability of linear regression models to fit highly nonlinear data is limited by the nature of the assumed regression model. For example, a quadratic model would provide a poor fit over a wide range to a data that has an exponential form. Since it is difficult to know the functional form of the data *a priori*, several regression models would have to be tried before a suitable model can be chosen. The automated regression analysis technique incorporated into DOE KISS affords us an opportunity to examine different interactions within a design to determine the most appropriate model. However, Deshpande, et al. (1997) and Subbarayan, et al. (1996) showed artificial neural network (ANN) models would provide a better approximation than a linear model since the problem surfaces in fatigue analysis are highly nonlinear. This is due to the mathematically proven ability of ANN models to fit arbitrarily complex functions. The use of ANN models is beyond the scope of the present study and a linear regression model will be used to get a general idea on how the fatigue life varies over the range of the factors.

4.3.4 Validation of Methodology

A hypothetical 2x2 area-array electronic assembly is used to validate the methodology. The material properties for this assembly are the same as those used for the 3-D electronic packages in Chapter 2. In this assembly, solder volume variation is assumed responsible for the variations in shapes of solder joints. The solder volume is varied linearly from the lower left corner of the assembly to the upper right corner as shown in Figure 4.3. By varying the volume in this manner, three out of the four solder joints had different shapes. The shape prediction program is then used to predict the final equilibrium configuration of the assembly. The equilibrium

configuration, shown in Figure 4.3 contained a package tilt of 1.77 degrees. A full three-dimensional finite element model of the warped assembly was also built and is shown in Figure 4.4. A side view of the warped assembly showing the package tilt is shown in Figure 4.5. The assembly is viewed from the lower right corner to the upper left corner. The cross-section of a nominal "ideal" assembly is shown in Figure 4.6.

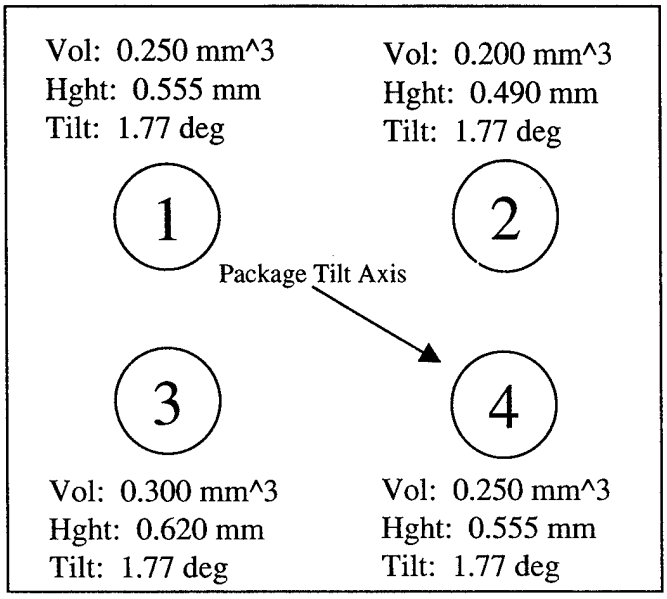

Figure 4.3 Equilibrium configuration with package tilt.

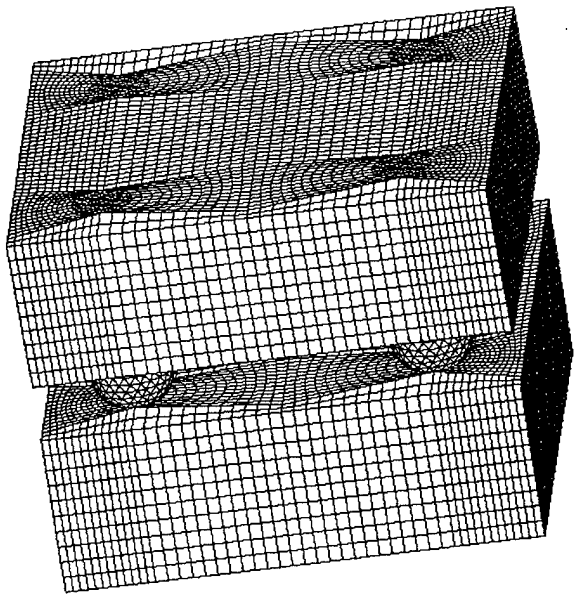

Figure 4.4 3-D model of the 2x2 assembly.

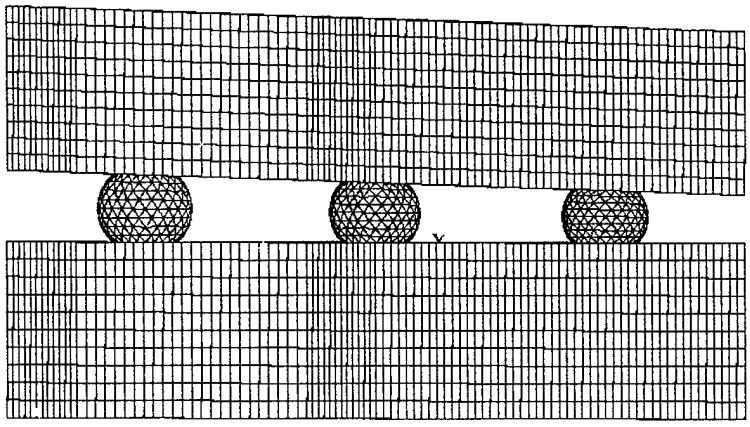

Figure 4.5 Side view of warped assembly.

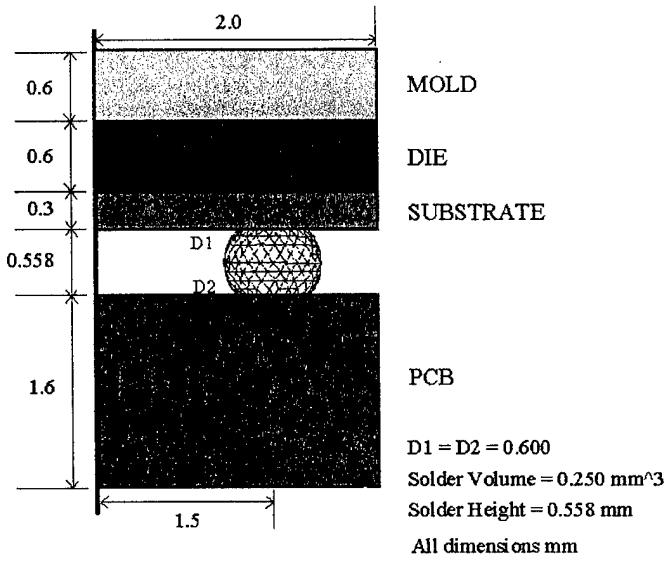

Figure 4.6 Cross-section of nominal assembly.

The full 3-D FE model of the 2x2 assembly was decomposed into linear and nonlinear sub-structures, package, PCB and solder. Superelements were generated from the 3-D FE models of the linear sub-structures, package and PCB, and using the work regression model for the non-linear sub-structure, solder, decomposition was used to analyze the assembly.

4.3.5 Results and Discussion

Table 4.5 shows the results of the analysis using the decomposed solution as compared to the finite element solution of the warped and nominal assemblies. Figure 4.7 shows the decomposition and FE relative shear displacement results and errors for the warped assembly. The 2x2 warped area-array model has an average displacement error of 12.57% across all four solder joints while the overall average relative shear

and axial displacement errors were 5.06% and 5.62% respectively. The 2x2 nominal area-array model has an average displacement error of 12.41% across all four solder joints while the overall average relative shear and axial errors were 5.51% and 4.70% respectively. The high average displacement errors can be attributed to our neglecting the work due to the local thermal mismatch at the solder interfaces. We showed in Chapter 2 that by including this analysis variable we were able to reduce the average error for the 225 I/O PBGA package by over thirty percent from 8.0% to 5.5%. It is reasonable to expect the same error reduction for the warpage study, however, as previously noted, solder reliability is based on the relative displacements and our relative displacement errors were very low. Due to symmetry, only one-quarter of the nominal package was analyzed using FE analysis.

Table 4.4 Results of decomposition analysis of warped assembly.

	Displacement Error (%)			Relative Displacement Error (%)	
	u	*v*	*w*	*shear*	*axial*
Warped Assembly					
Component	17.84	18.08	13.18	5.06	5.62
PWB	4.86	4.69	16.77		
		Average	**12.57**		
Nominal Assembly					
Component	17.86	18.06	13.21	5.51	4.70
PWB	4.56	4.34	16.46		
		Average	**12.41**		

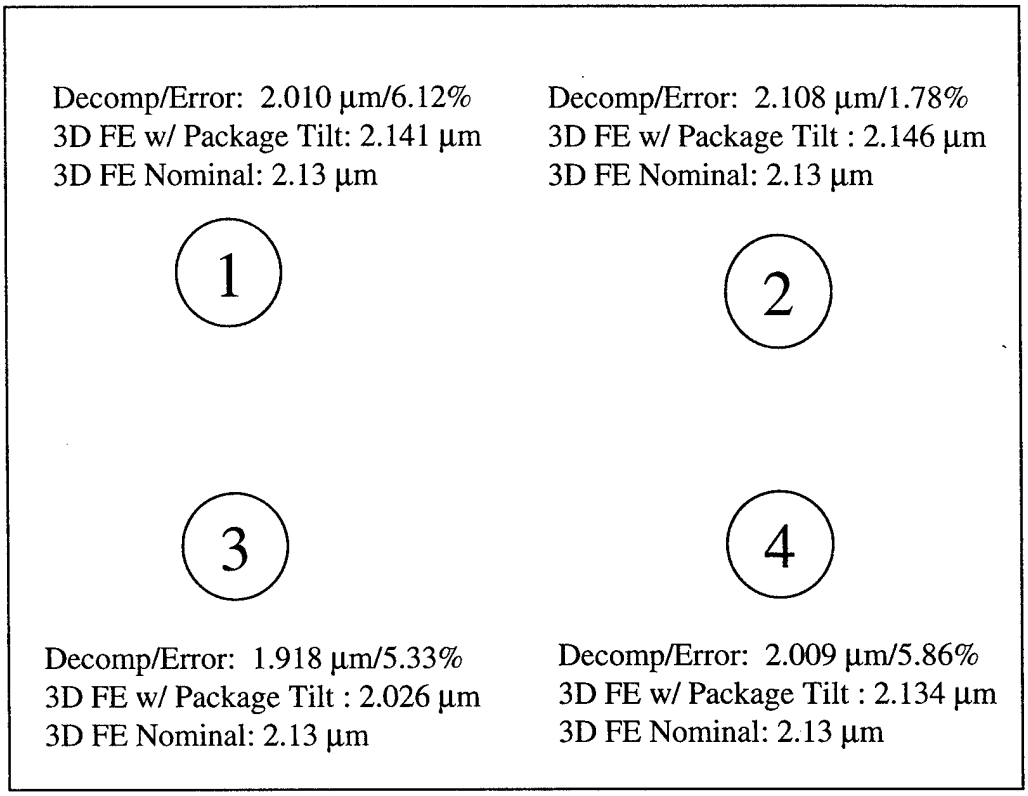

Figure 4.7 Relative shear displacements and errors.

A reliability study was completed to study the affect of warpage on solder joint reliability. The study compared results of the decomposition and FE modeling. Critical to this study was the effect of the neglecting package tilt on solder joint reliability. To accomplish this, the package tilt parameters in the solder shape program were turned off and the package reanalyzed to find the equilibrium configuration. Figure 4.8 depicts the equilibrium configuration without package tilt. Additionally, relative shear displacements for FE model without package tilt were assumed the same as those for the FE model with package tilt. Results of the reliability study are shown in Figures 4.9 and 4.10. The percent errors in Figure 4.9 are based on the decomposition and FE results of the 2x2 hypothetical model with package tilt.

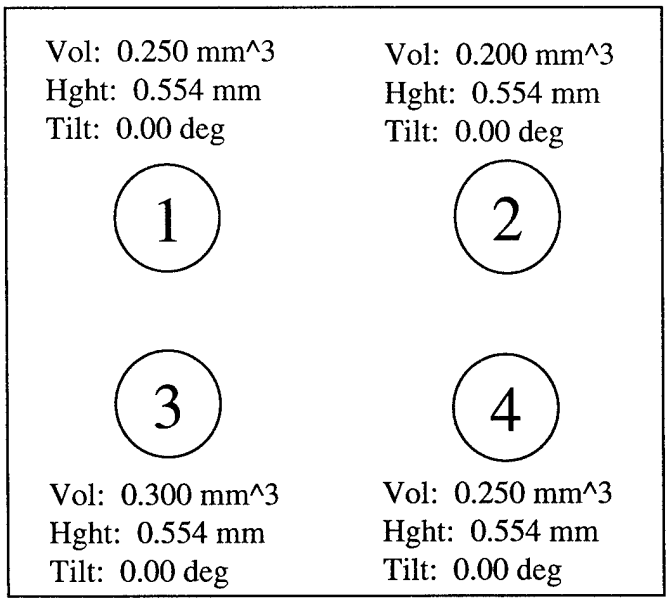

Figure 4.8 Equilibrium configuration without package tilt.

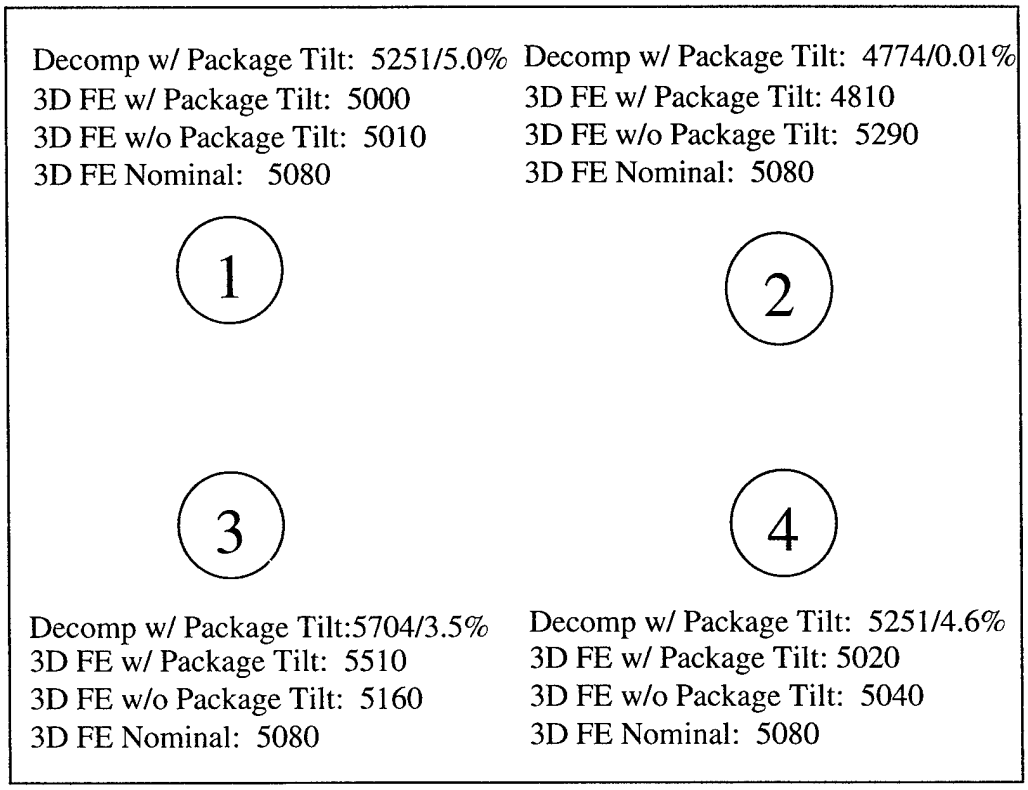

Figure 4.9 Results of reliability study (cycles to failure).

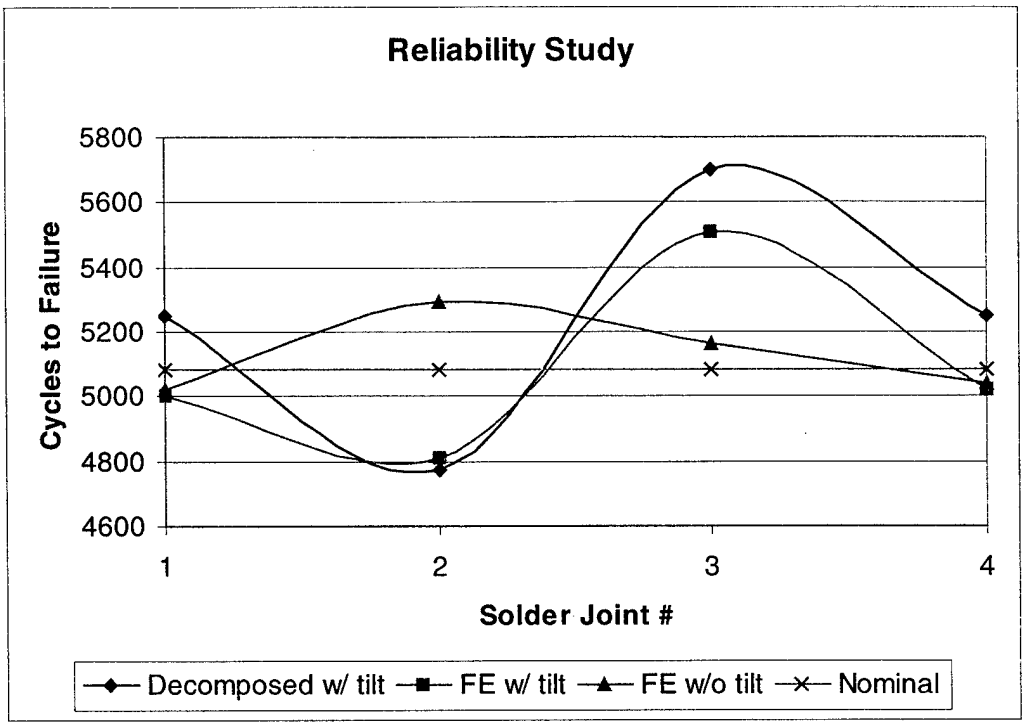

Figure 4.10 Cycles to failure plot.

As seen in Figure 4.10, for this hypothetical package, failure to include package tilt in determining the equilibrium of warped electronic assemblies can result in errors in reliability estimates by as much as 10 percent. The reason for this error is volume variation in the assembly caused the package to tilt, which directly affected the standoff height of the solder joints. Chan, et al. (1997) showed in their study that fatigue life is strongly dependent on the height of solder joint. This is a critical finding because as electronic packages continue to grow in size, warpage and its effect of package tilt will increase in importance, and ignoring tilt would lead to large errors in reliability. For example, an 1140 I/O Flip Chip Ball Grid Array (FCBGA) electronic package shown in Figure 4.11 has a diagonal length of 26.9 mm. The package has a 500 micron nominal solder joint height and the solder ball array is peripherally distributed. A package of this type would only need a 1.065 degree tilt at

the center to make the edge of the package incident on the PCB. We must note the volume variation in our hypothetical package was deliberately chosen to be extreme to properly demonstrate the methodology. We would not expect to find such a volume distribution in "real-world" electronic packages, however, arbitrary, non-symmetric warpage of PCBs and packages is a major concern in the electronic packaging industry, and we showed in Chapter 3 warpage of this type could cause the package to tilt. The FCBGA package above would not require such an extreme volume variation or arbitrary warpage to achieve a 1.065 degree package tilt.

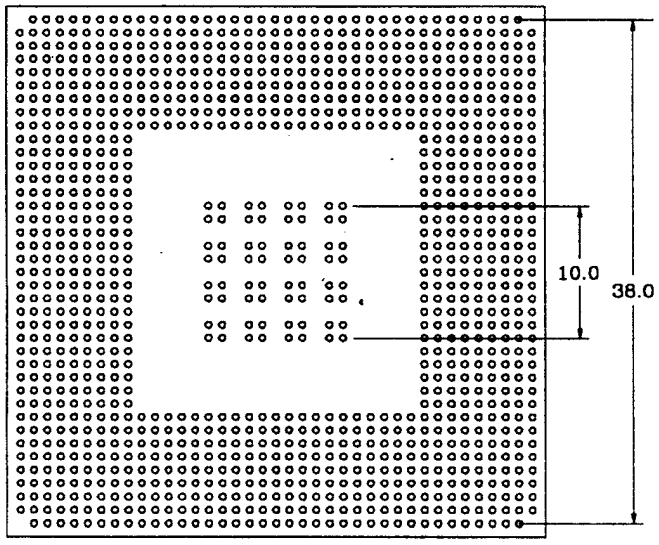

Figure 4.11 1140 I/O Flip Chip Ball Grid Array Package.

Lastly, using the regression model for solder work, Equation 4.1, plots of the interactions between the design/manufacturing variables, volume, height and warpage, and analysis variable, relative shear (Figures 4.12 – 4.14), show the interactions between height and shear and warpage and shear to be negligible. The absence of interaction is evident in the parallel running of the lines. There is a small interaction between volume and shear, however, for this study the solder volume distribution was

extreme to demonstrate the methodology. As stated previously, we would not find such a volume distribution in a "real-work" electronic package. This suggests that the assembly design/manufacturing parameters (solder volume, height, and warpage) do not significantly influence the relative displacements on the solder joints. Further, a comparison of the FE relative shear displacements for the hypothetical warped and nominal area-array assemblies, as shown in Figure 4.7, produced a maximum relative shear displacement error of 5.13 percent at solder joint #3. That is, the package tilt does not significantly alter the displacements in this particular package. Therefore, it is reasonable to assume that the analysis of nominal area-array assemblies is all that is needed to determine the assembly equilibrium configuration during temperature cycling. The relative shear displacements from these analyses are sufficient for subsequent solder joint reliability studies.

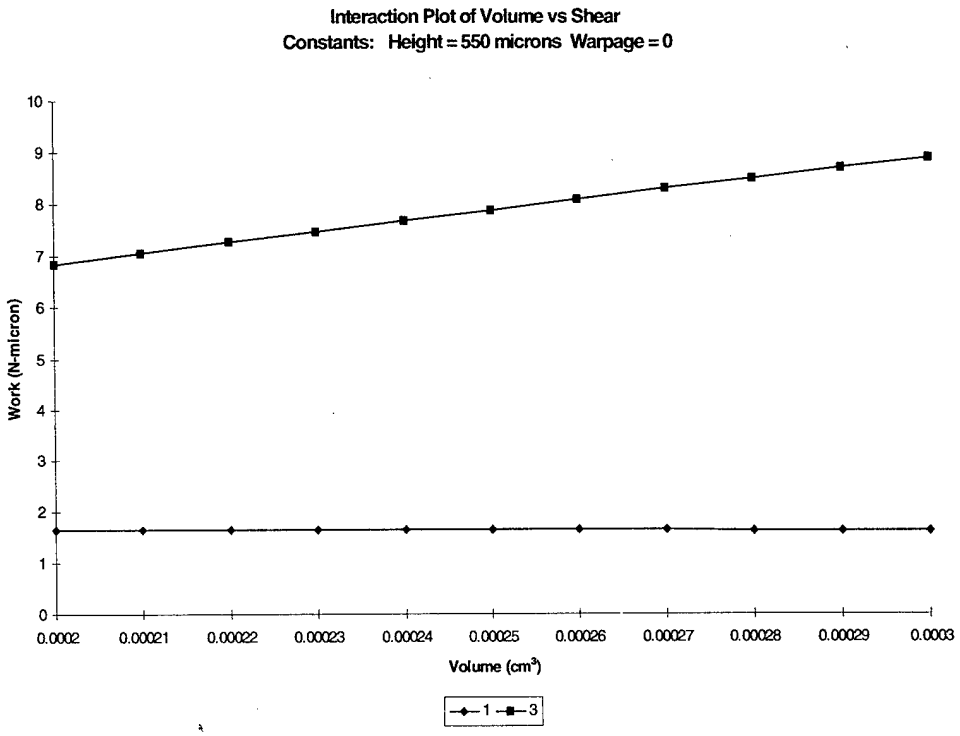

Figure 4.12. Interaction plot of volume vs. shear.

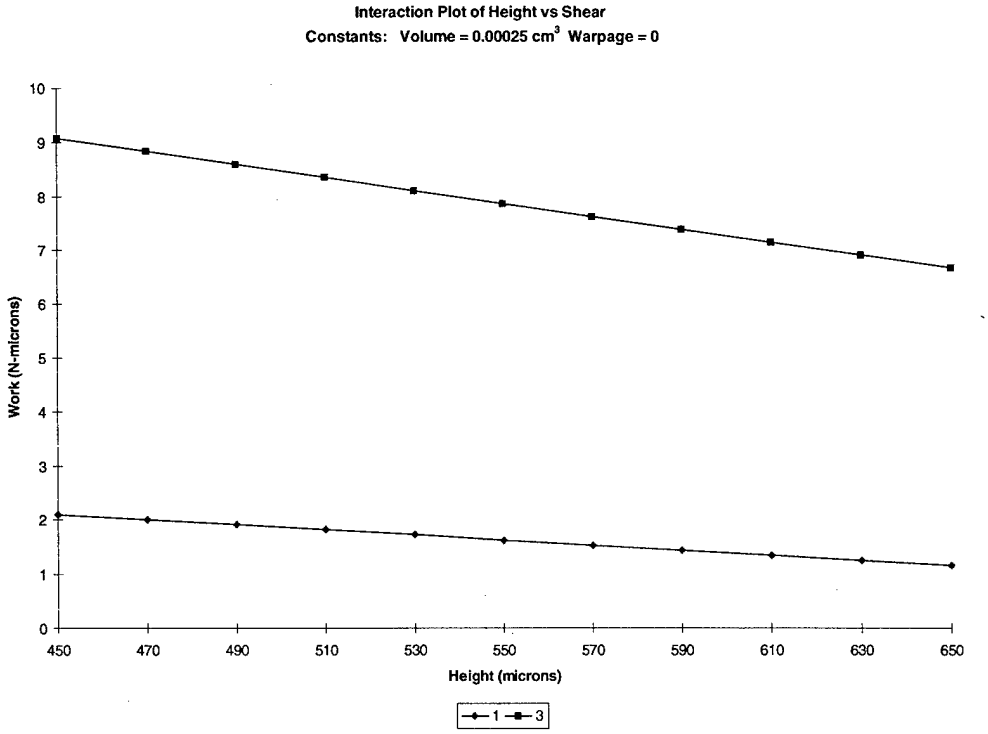

Figure 4.13 Interaction plot of height vs. shear.

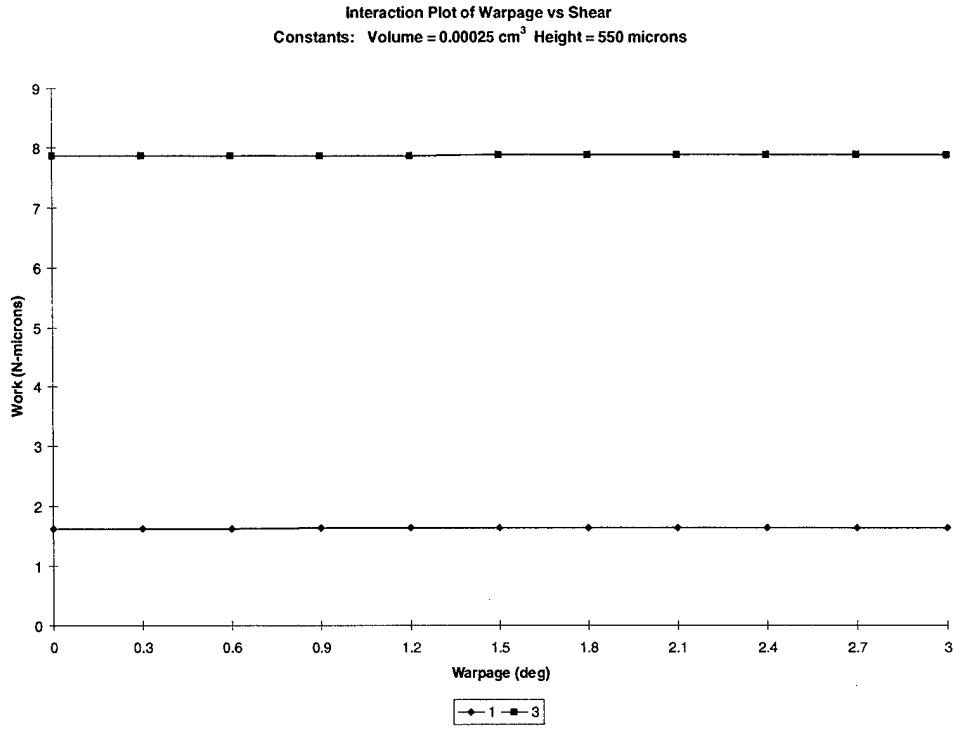

Figure 4.14 Interaction plot of warpage vs. shear.

3-D surface plots of the linear regression model for solder fatigue life (Equation 4.5) provide important insight into the effect of warpage on solder joint reliability. A pad tilt caused by warpage can affect reliability in two ways: due to a changed standoff height (and its subsequent effect on stresses) or due to the change in the nature of singularity at the joint/PCB or the joint/component interface. A plot of solder height versus pad tilt due to warpage (Figure 4.15) shows solder pad tilt caused by warpage independent of solder standoff height does not affect reliability. That is, the nature of the singularity is not significantly altered by the pad tilt. A plot of solder volume versus height (Figure 4.16) shows that as the shape of the solder changes from convex (truncated sphere) to concave (hour-glass) the fatigue life of the solder joint increases. The main reason for this change in reliability versus

solder shape change is because the inelastic dissipation is concentrated at the location having the smallest cross-section. In addition, convex (truncated sphere) solder joint have higher strain energy density due to the acute contact angle at the solder/package and solder/PCB interfaces causing (elastically) singular stress fields. As shape changes from convex to concave (hour-glass shaped) the interfacial contact angle increases reducing the stress concentrations (Deshpande, et al, 1997). This can be seen in Figures 4.17 – 4.20 which show the plastic dissipation contours of a solder joint with a prescribed volume (2.5 E-4 cm^3), fixed relative shear displacement (2.0 microns), and prescribed pad diameters (600 microns). The height of the solder joint varies from 500 to 1100 microns, as is necessary to produce convex and concave shapes. For a convex (truncated sphere) shaped solder joint (Figure 4.17) with low interfacial contact angle (high curvature), the highest plastic dissipation value is approximately 0.3661 MPa and is located at the pad interfaces. For a barrel-shaped solder (Figure 4.18), with increased interfacial contact angle, the highest strain energy density value is approximately 0.3457 MPa and is located at the pad interfaces. For a cylindrical shaped solder (Figure 4.19), with a further increase in interfacial contact angle, the highest strain energy density value is approximately 0.1740 MPa and is located at the pad interfaces. Lastly, for a concave (hour-glass) shaped solder (Figure 4.20), with maximum interfacial contact angle (low curvature), the highest strain energy density value is approximately 0.1153 MPa and is located close to the center of the solder joint where the cross-section area is smallest. This study confirms the results of the studies by Ju, et al. (1994, Chan, et al. (1997), and Deshpande, et al. (1997).

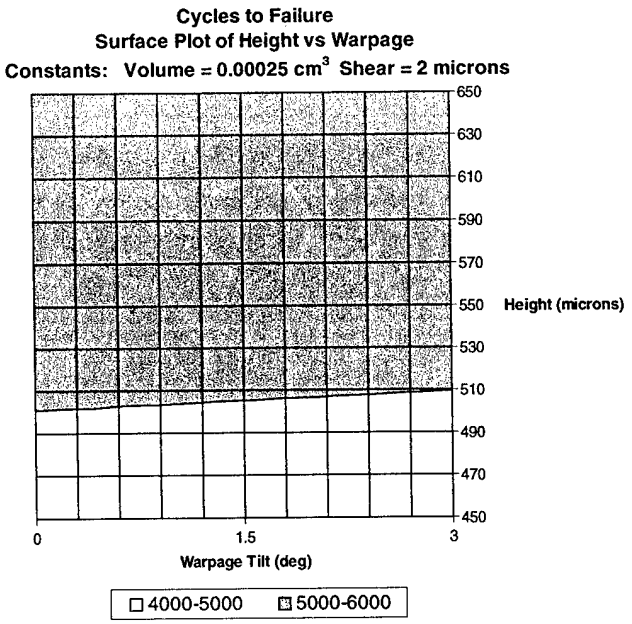

Figure 4.15 Cycles to failure surface plot of height vs. warpage.

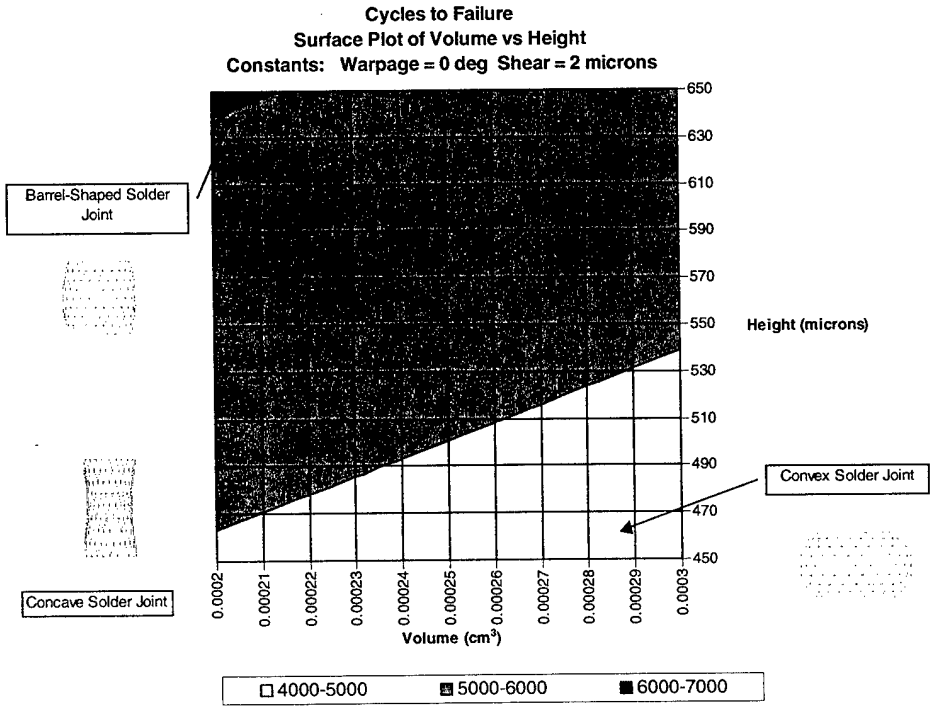

Figure 4.16 Cycles to failure surface plot of volume vs. height.

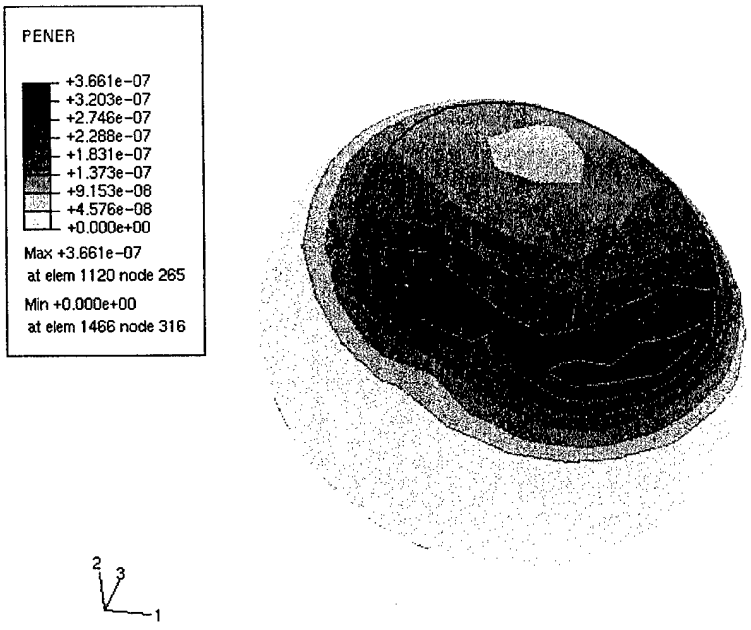

Figure 4.17 Plastic dissipation density plot for convex (truncated) solder joint.

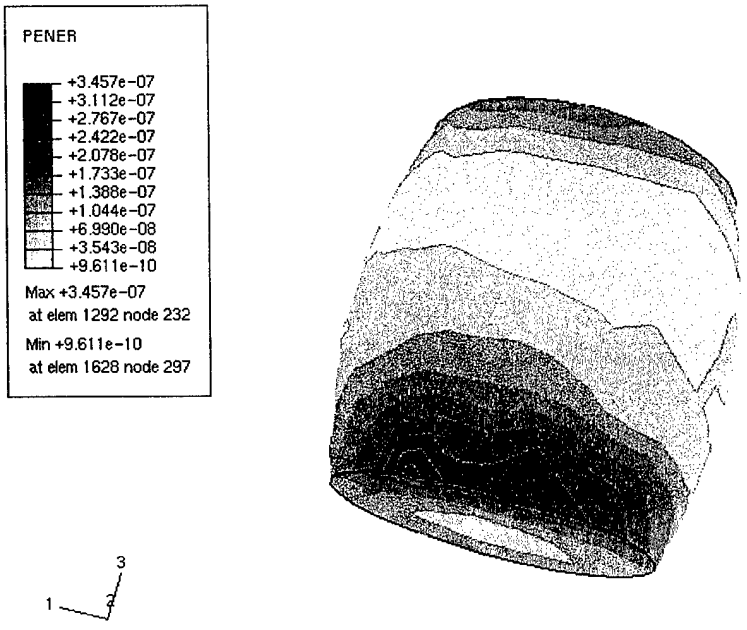

Figure 4.18 Plastic dissipation density plot for barrel-shaped solder joint.

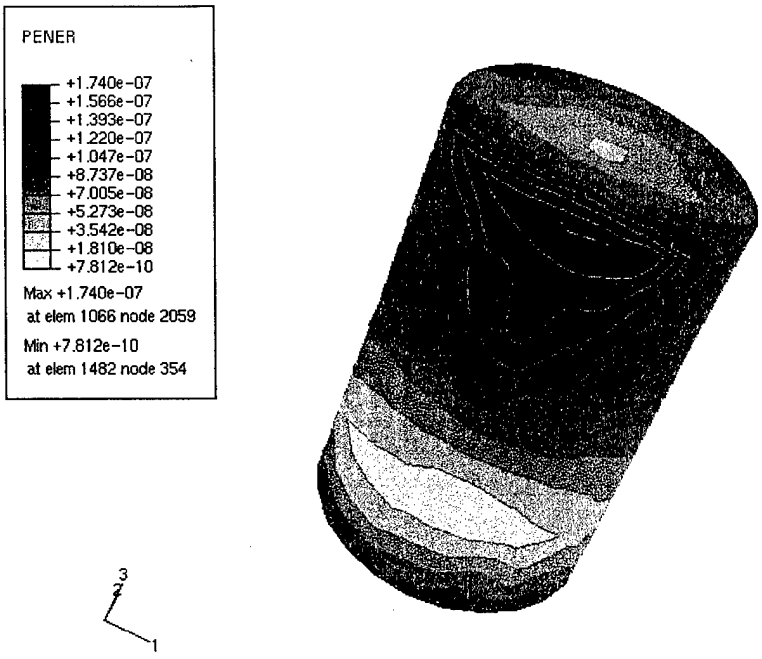

Figure 4.19 Plastic dissipation density plot for cylindrical solder joint.

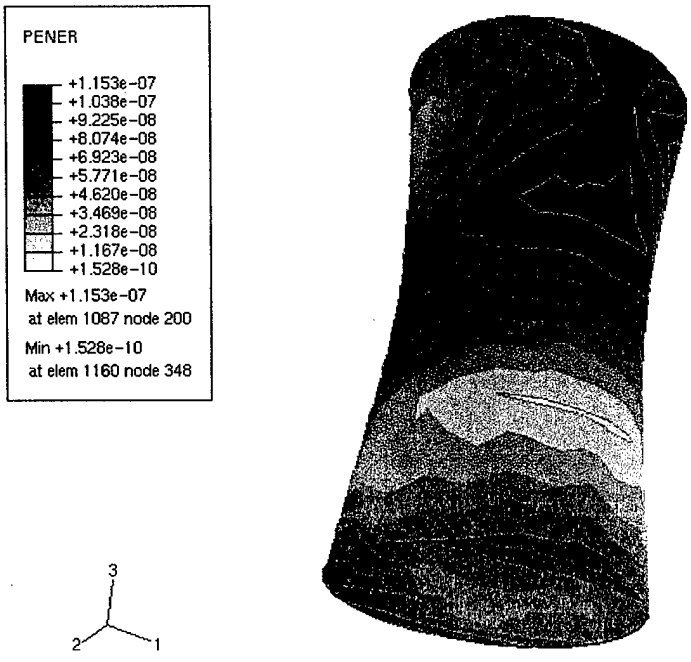

Figure 4.20 Plastic dissipation density plot for concave (hour-glass) solder joint.

For the 2x2 warped assembly, the shape of the solder joint ranged from concave to barrel-shaped (See Figure 4.16). Lastly, Figure 4.21 shows how a combined bowl-type warpage of the assembly can be enhanced. The dotted line indicates the cycles to failure path for an arch-type warpage. The fatigue life ranges from 8000-10000 cycles for solder joints located close to the neutral point (low relative shear) of the assembly to 2000-4000 cycles for solder joints located far away from the assembly neutral point (high relative shear). The solid line indicates the cycles to failure path for a combined bowl-type assembly warpage. The fatigue life ranges from 6000-8000 cycles for solder joints located close to the assembly neutral point to 0-2000 cycles for joints located far away from the neutral point. Therefore, depending on the type of package warpage, the fatigue life at solder joints with high relative shear can change by over 200 percent. This agrees with the findings of Chan, et al. (1997).

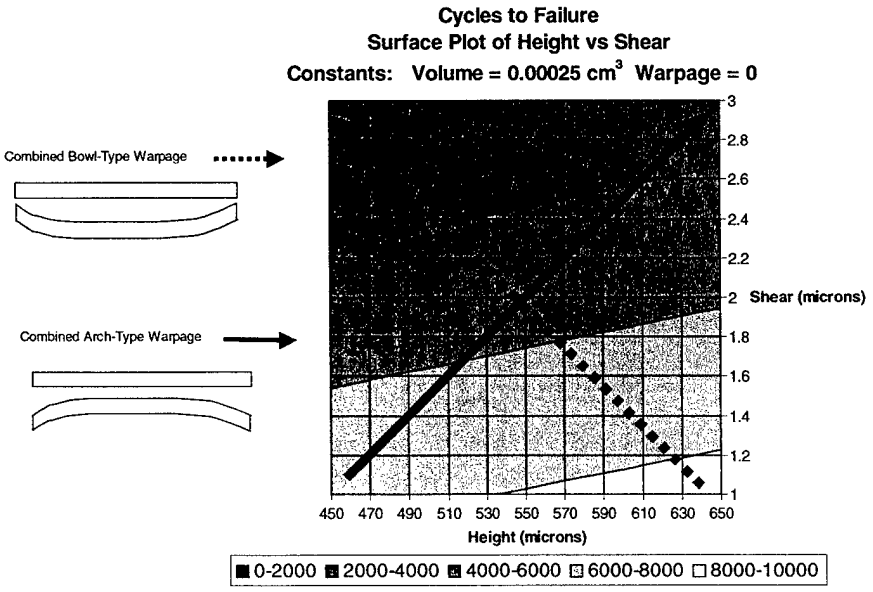

Figure 4.21 Cycles to failure surface plot of height vs. shear.

4.4 Conclusions

A novel procedure is developed for analysis of area-array solder joint reliability. The model consists of three steps: 1) calculation of solder shapes using novel package configuration prediction methodology, 2) calculation of stresses/strains and cyclic inelastic dissipations using a decomposition modeling technique, and 3) estimation of solder joint fatigue life using a regression model for fatigue life. Fatigue life calculation was based on a modified Darveaux relationship (Darveaux, et al., 1995). It is shown that the decomposed solution methodology results in an overall accuracy loss in relative shear displacements of approximately 5.06 percent when compared with a full finite element model. This displacement error leads to an error in fatigue life of approximately 3.28 percent due to incorrectly calculated inelastic dissipation. A comparison of the reliability of a package with warped and non-warped joints reveals package tilt due to solder volume variation and/or non-symmetric warpage can change the stand-off height of solder joints significantly affecting solder joint reliability. However, we found that individual solder pad tilts, independent of their effect on standoff height, do not affect the reliability of solder joints.

Chapter 5

Conclusions and Recommendations

5.1 Conclusions

During the course of the research presented in this thesis, a novel methodology for assessing the reliability of warped solder joints in area-array electronic packages was developed. The methodology is incorporated into the three basic and critical steps to determine package reliability:

1. calculate solder joint shapes,
2. calculate thermal stress/strain distribution in the most susceptible joint after solidification and during thermal cycling, and
3. assess solder joint reliability.

For step one, a novel methodology was developed to determine the final equilibrium configuration of an area-array package. The novel techniques in this methodology include;

⇒ First application of homogeneous transformation theory to predict the equilibrium configuration of electronic packages

- ♦ First use of rigid rotations of package

⇒ Methodology is capable of predicting equilibrium in presence of arbitrary warpage

For step two, a decomposed analysis procedure is successfully implemented to determine the deformation of area-array assemblies with warped solder joints, a novel application of this procedure. In addition, analysis of 2-D and 3-D hypothetical and "real-world" warped and non-warped electronic packages produced the following:

⇒ Refined model for solder response through additional basis terms

⇒ Successfully demonstrated methodology on "real-world" electronic package with non-warped solder joints

⇒ Successfully demonstrated methodology on hypothetical electronic package with warped solder joints

⇒ Provided insight into decomposed approach

- Displacement versus relative displacement errors

⇒ Provided insight into energy contributions to relative displacement errors

⇒ Led to assumption that the analysis of a nominal area-array assembly is all that is required to obtain the displacements required to assess reliability of individual, warped solder joints.

For step three, our study showed the following:

⇒ Solder pad tilt in a range of 0 to 3 degrees, independent of its effect on solder stand-off height, has a negligible effect on solder joint reliability

⇒ Package tilt due to solder volume variation and/or arbitrary package or PCB warpage can change the stand-off height of solder significantly affecting solder joint reliability

- We found a reliability calculation error as high as 10 percent for the 2x2 hypothetical array

5.2 Recommendations

The results of the research successfully demonstrate the power of the decomposition analysis procedure and the novel methodology for determining the equilibrium configuration of area-array packages during solder reflow. As with any new technique, additional research must be accomplished before the technique can be accepted as state-of-the-art and become an industry standard analysis technique like finite element analysis. The following is a list of recommendations for future studies related to the work presented in this thesis:

5.2.1 Decomposition

⇒ Generate solution for high relative displacement errors attributed to superelement energy contribution

⇒ Incorporate time-dependent (creep) behavior into solder work model

⇒ Demonstrate methodology on a "real-world" warped electronic package

- Verify assumption that the decomposed analysis of nominal area-array assemblies is all that is needed to determine package equilibrium during temperature cycling

- This is based on the low relative displacement errors between FE analysis of hypothetical assemblies with warped and non-warped solder joints and the negligible manufacturing and analysis variable interactions discovered during regression analysis of designed experiments

⇒ Use decomposition to determine optimal construction of area-array packages

⇒ Produce Windows/Unix based user-friendly program utilizing this methodology

5.2.2 Solder Shape Prediction

⇒ Incorporate pad off-set into shape prediction modeling

⇒ Demonstrate procedure on "real-world" electronic package

⇒ Use solder shape prediction program as a tool to predict solder joint yield during solder reflow

5.2.3 Fatigue Life Calculation

⇒ Assess reliability of warped solder joints in the presence of pad-offset

Bibliography

ABAQUS User's Manual, Version 5.7, Hibbit, Karlsson & Sorensen Inc.,Pawtucket,RI, 1997.

Amagai, Masazumi, "Characterization of Molding Compounds and Die Attach Materials for Package Warpage and Solder Joint Reliability in Chip Scale Packages (CSP)," ASME Advances in Electronic Packaging, Vol. 2, pp. 1103-1112, 1999.

Barker, D.B., Gupta, V.K. and Cluff, D., "Solder Joint Crack Initiation and Crack Propagation in A TSOP using Strain Energy Partitioning," ASME Advances in Electronic Packaging, EEP-Vol. 4-2, pp. 943-949, 1993.

Borgessen, P., Li, C.Y., and Conway, H.D., "Analytical Estimates of Thermally Induced Stresses and Strains in Flip-Chip Solder Joints," ASME Advances in Electronic Packaging, EEP-Vol. 1-2, pp. 845-854, 1992.

Brakke, K.A., *Surface Evolver Manual, Version 1.94*, Minneapolis, MN: Univ. of Minnesota Press, Jan 94.

Chan, Y.W., et al., "Reliability Modeling for Ball Grid Array Assembly with a Large Number of Warpage Affected Solder Joints," ASME Advances in Electronic Packaging, Vol. 2, pp 1507-1514, 1997.

Corbin, J.S., "Finite Element Analysis for Solder Ball Connect (SBC): Structural Design Optimization," IBM Journal of Research and Development, Vol. 37, No. 5, pp. 585-596, 1993.

Craig, J.J., "Introduction to Robotics: Mechanics and Control," Addison-Wesley, Reading, MA, 1989.

Darveaux, R., Banerji, K., Mawer, A., and Doddy, G., "Reliability of Plastic Ball Grid Array Assembly," *Ball Grid Array Technology*, J. H. Lau, ed., McGraw-Hill, Inc., New York, 1995.

Deshpande, A., Subbarayan, G., and Mahajan, R., "Maximizing Solder Joint Reliability Through Optimal Shape Design," ASME Journal of Electronic Packaging, Vol. 119, pp. 149-155, September, 1997.

Deshpande, A., Subbarayan, G., and Rose, D., "A System for First Order Reliability Estimation Of Solder Joints In Area Array Packages," Presented at the 1998 ASME International Mechanical Engineering Congress and Exhibition, Nov. 15-21, Anaheim, CA, 1998.

Deshpande, A. and Subbarayan, G., "Decomposition Techniques for the Efficient Analysis of Area-Array Packages ASME Journal of Electronic Packaging, Vol. 1, pp. 13-20, March 2000.

Digital Computations, Inc., User's Guide, *DOE – KISS*, Colorado Springs, CO, Air Academy Press and Associates, LLC, 1997.

Farhat C., and Crivelli L., "A General Approach to Nonlinear FE Computations on Shared-Memory Multiprocessors," Computer Methods in Applied Mechanics and Engineering, Vol. 72, No.2, pp.153-71, 1989.

Farhat C., and Wilson E., "A New Finite Element Concurrent Computer Program Architecture," International Journal for Numerical Methods in Engineering, Vol. 24, pp. 1771-1792, 1987.

Haftka, R.T., and Gurdal, Z., "Elements of Structural Optimization," Kluwer Academic Publications, Dordrecht, The Netherlands, 1992.

Heinrich, S.M. and Lee, P.S., "Solder Geometry Prediction in Electronic Packaging: An Overview," EEP-vol. 19-2, ASME Advances in Electronics Packaging, 1997.

IDEAS User's Manual, Version 8.0, Structural Dynamics Research Corporation Inc., Milford, OH, 2000.

Lau, J.H. and Rice, D.W., "Thermal Fatigue Life Prediction in Flip Chip Solder Joint by Fracture Mechanics Method," ASME Advances in Electronic Packaging, EEP-Vol. 1-1, pp. 385 -392, 1992.

Li Y., and Mahajan, R.L., "CBGA Solder Fillet Shape Prediction and Design Optimization," ASME Journal of Electronic Packaging, Vol. 120, pp. 118-122, 1998.

Montgomery, Douglas C., Introduction to Statistical Quality Control, 3rd Edition, John Wiley & Sons, New York, 1997.

Mortenson, M.E., "Geometric Modeling," 2nd Edition, John Wiley and Sons, Inc., New York, 1997.

Nagaraj, B., and Mahalingam, M., "Package-to-Board Attach Reliability – Methodology and Case Study on OMPAC Package," ASME Advances in Electronic Packaging, EEP-Vol. 4-1, pp. 537-543, 1993.

Peace, G.S., *Taguchi Methods: A Hands-On Approach*, Addison-Wesley, Reading, MA, 1993.

Renken and Subbarayan, "NURBS-Based Solutions to Inverse Boundary Problems in Droplet Shape Prediction," in press, Computer Methods in Applied Mechanics and Engineering, 2000

Schittkowski, K., "NLPQL: A Fortran subroutine solving constrained nonlinear programming problems," Annals of Operations Research, Vol.5, pp.485-500, 1985/6.

SIA, "The National Technology Roadmap for Semiconductors," 1997.

Subbarayan, G., "A Procedure for Automated Shape and Life Prediction in Flip-Chip and BGA Solder Joints," ASME Journal of Electronic Packaging, Vol. 118, pp. 127-133, 1996.

Subbarayan, G., et al., "Reliability Simulations for Solder Joints Using Stochastic Finite Element and Artificial Neural Network Models," ASME Journal of Electronic Packaging, Vol. 118, 1996.

Sutherline, W., et al., "A Relative Comparison of PWB Warpage due to Simulated Infrared and Wave Soldering Processes," 1998 Electronic Components and Technology Conference, pp 807-815, 1998.

Tower, Susan, et al., "Yield Prediction for Flip-Chip Solder Assemblies Based on Solder Shape Modeling," IEEE Transactions on Electronic Packaging Manufacturing, Vol. 22, No. 1, pp 29-37, Jan 1999.

Wong, T.E., Cohen, H.M., Jue, T.Y., and Teshiba, K.T., "Ceramic Ball Grid Array Solder Joint Thermal Fatigue Life Prediction Model," ASME Advances in Electronic Packaging, EEP-Vol. 26-1, pp. 427-432, 1999.

Zhang, L., Hunter, B., Subbarayan, G., and Rose, D., "The Accuracy of Structural Approximations Employed in Analysis of Area Array Packages," IEEE Transactions Components and Packaging Technology, Vol. 22, No. 4, December, 1999.

Zhao, J.-H., Dai, X., and Ho, P.S., "Analysis and Modeling Verification for Thermal-Mechanical Deformation in Flip-Chip Packages," 1998 Electronic Components and Technology Conference, pp 336-343, 1998.

Zienkiewicz, O.C. and Taylor, R.L., *The Finite Element Method. Volume 1.* McGraw-Hill, London, 1989